CHAPTER 2

Experimental techniques and theoretical background

2.1. Introduction

This chapter deals with the detailed description of several experimental techniques employed, relevant operational principles, mathematical expressions and theories in connection with the study to perform the experiment. Theoretical discussions associated with mesophase transitions in liquid crystals those are related to the subject matter of this dissertation are also included in this chapter.

2.2. Experimental techniques

2.2.1. Liquid crystal cells and sample preparation

To investigate different physical properties of Liquid Crystal (LC) sample, it is necessary to prepare a proper alignment and uniform ordering. The crystalline property of the liquid crystal material is developed when it is considered as a smaller sized ordered domain. It is possible to obtain such small domains when the sample is taken sandwiched in between two glass slides, *i.e.*, when it becomes a thin layer. However, to investigate some higher order mesophases, the perfect alignment of molecules is required within the glass substrates. Such alignment can be achieved by using LC cells whose walls are treated with polyimide coating (for surface anchoring) and ITO coating (for application of external electric field) in a variety of ways to accomplish different molecular alignments. Examples of those alignment cells are – (i) homogeneous (HG) or planar cell where molecular long axes are directed parallel to the glass surface, (ii) homeotropic (HT) cell where molecular long axes are aligned perpendicular to the glass surface, (iii) tilted LC cell where the molecular long axis is tilted with respect to the surface normal, (iv) hybrid cell in which the molecules are parallel to one substrate and perpendicular to another substrate etc. Among them, only commercially available (AWAT PPW, Warsaw, Poland) HG and HT cells (Fig. 2.1) of

suitable thickness were used in different experiments related to this dissertation.

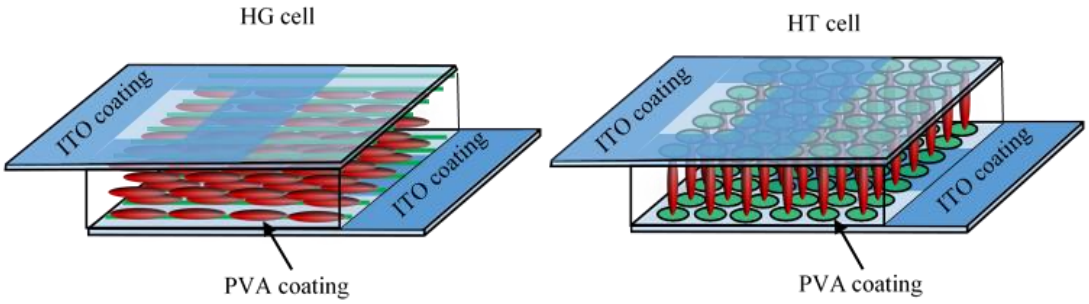

Figure 2.1. Orientations of the molecules in planar (HG) and homeotropic (HT) cells.

In order to improve different physical properties of LC materials for application purpose and also for the investigation of transitional phenomena at different mesophase transition, it is often required to formulate some binary or multi-component mixtures rather than investigating the pure compounds. Therefore, the two or more pure LC compounds were taken in a vial with particular proportion after carefully weighting it in a high precision digital balance (Mettler Toledo AB-265-S) and then mixed them by placing the vial in a continuous shaker machine or often placed in an ultrasonicator (SONAPROS PR 250-MP) for several hours at a fixed temperature close to their clearing temperatures. After preparation of homogenous mixture, samples were filled up in LC cells of suitable thickness and alignment by the capillary action and proceeds further for experimental studies.

2.2.2. Texture study

Optical textures of liquid crystal sample are the appearance of some characteristic visual pattern when viewed under a crossed polarizing microscope probed with a polarized light. Such appearance is due to the defect structure of long-range molecular ordering for liquid crystal samples. Visualization of these optical textures are different for different mesophases, details descriptions are available in the literature [1,2]. Therefore, the texture

observation is the preliminary tool to characterize different mesophases and their phase transition temperatures which helps further to construct a phase diagram of binary mixtures by varying the concentration of guest LC compound.

Texture observation were made by taking a small amount of sample in a glass slide and covered it by a small cover slip over the sample to make a thin layer and often filled the sample in commercially available LC cells. These slides/cells were kept in a hot/cooling stage (HCS302) made by INSTEC equipped with a programmable temperature controller mK1000 (INSTEC). The mesophase textures in the entire mesomorphic range were observed under polarizing optical microscope BANBROS BPL400 B attached with a CCD camera Moticam 580 (5.0 MP).

2.2.3. Differential scanning calorimetry (DSC)

In order to detect the actual phase transition temperature of mesophases, the differential scanning calorimetry or DSC study is complementary technique to polarizing optical microscopy. DSC measurement reveals the presence of mesophases by detecting the enthalpy change associated with the phase transitions. It is also capable of identifying the order nature of phase transitions by variation of temperature [3-5]. Although this measurement cannot identify the type of phases, it provides some useful information about the conformational disorder [6], purity of the sample [7], order of the phase transitions [3-5] etc.

Investigation on DSC study for some LC samples related to this dissertation was carried out by Pyris Diamond Perkin-Elmer 7 [8], Institute of Physics, Academy of Sciences of the Czech Republic, 18221 Prague, Czech Republic. The sample of amount 4 mg was hermetically sealed in an aluminium pan and proceeds further to heat/cool in a nitrogen atmosphere at a heating/cooling rate of 10 $^{\circ}$C per minute. The temperature and the enthalpy change [ΔH] were calibrated on the extrapolated onsets of melting points of

ice, indium and zinc. The details procedure to determine the transition temperature and corresponding enthalpy changes have been described by Ratna *et al.* [9].

2.2.4. Optical birefringence measurement

The liquid crystal materials possess an optical anisotropy due to the existence of shape anisotropy of the constituent molecules and relative orientation of the molecular director with respect to the direction of light propagation. If the direction of the incident light beam (polarized) is perpendicular to the direction of the molecular optic axis, the refracted light beam splits into an ordinary refractive index (n_o) along with an extraordinary refractive index (n_e), directed perpendicular and parallel to the molecular optic axis respectively. Hence, it is well known as "doubled refraction". Both the refracted light beam is plane polarized and orthogonal to each other. However, the birefringence (Δn) is the difference of those refractive indices and can be defined as:

$$\Delta n = n_e - n_o \tag{2.1}$$

The optical birefringence of liquid crystal compounds have been determined in this dissertation by two different methods: (i) the thin prism method [10,11], where both n_o and n_e has been measured directly from sample filled thin prism by variation of temperature and (ii) the high-resolution optical transmission technique [12-16], where the birefringence has been measured by probing the temperature dependent phase retardation at different mesophases of liquid crystal materials filled in LC cells.

a. Thin prism technique

In the thin prism technique, the LC sample has been inserted within a lab-made hollow prism of prism angle less than 2°. This kind of prisms were constructed by two pieces of glass slide having dimension 2×3 cm and 2×2 cm and a thin glass spacer was introduced between them at one end of the vertical

edges to achieve the prism angle less than 2°. Glass slides were treated for one hour with an acid mixture (conc. HNO_3 and conc. H_2SO_4) at a temperature of about 60 °C. After washing the glass slides with distilled water, treated further with 1 molar solution of KOH for several hours. They were the rinsed thoroughly with distilled water for several times and left in acetone for few hours to remove any residual impurity. Furthermore, to obtain a homogeneous molecular alignment, a thin layer of dilute polyvinyl alcohol was applied to contact surfaces of the glass slides and the dry surfaces were uniformly rubbed for several times with a filter paper. The glass plates were then sealed by using a high temperature adhesive. Next the prisms were baked in an oven at about 100 °C for several hours. However, before introducing the LC samples, the refracting angle of the prisms were determined by filling with ultrapure water and measuring the deviation produced in LASER beam.

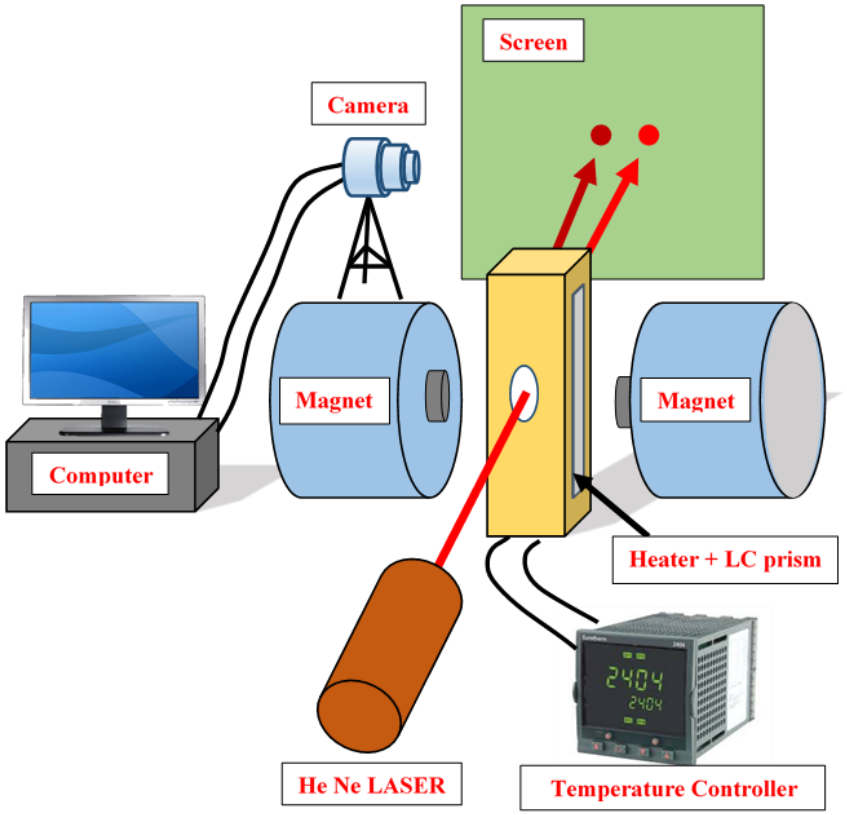

Figure 2.2. Schematic diagram of the experimental set-up for refractive index measurement.

An experimental set-up designed (Fig. 2.2) in such a way that a LASER beam of wavelength λ = 632.8 nm (He-Ne laser made by Thorlab) can pass through the sample filled prism placed within a brass made heater, temperature of which was controlled by a temperature controller Eurotherm PID 2404 with an accuracy of ±0.1 °C. The heater containing LC filled prism was placed in between two pole pieces of an electromagnet by which a magnetic field of about 1T can be applied to align the sample. After passing through the prism the incident light beam splits into the ordinary and extraordinary components and produces two spots on a white screen at a fixed distance (d). The images of such visual spots were recorded by a digital camera suitably interfaced with a computer. Moreover, by locating the center of the recorded spots, the temperature variation of ordinary (n_o) and extraordinary (n_e) refractive indices and hence the average refractive index $n_{av} = \sqrt{\{(2n_o^2+n_e^2)/3\}}$ along with birefringence (Δn) has been determined by this technique with an accuracy of ±0.0006.

b. Optical transmission technique

In order to obtain the precise value of optical birefringence (Δn), the optical transmission (OT) technique [14-21] has been accomplished in which the intensity of a LASER beam transmitted through a liquid crystal filled cell and corresponding phase retardation ($\Delta\varphi$) has been measured. A high-intensity LASER beam of wavelength λ = 532 nm (or 632.8 nm) was projected on a planar aligned sample filled LC cell, placed in between two crossed analyzer and polarizer (Glan-Thomson). The LC cell was placed in a brass made heater, the temperature of which was controlled and measured by a temperature controller Eurotherm PID 2404 with an accuracy of ±0.1 °C. Additionally, to obtain better thermal stability in the experiment, a two stage heating arrangement was employed by placing the heater inside of a big heating/cooling oven which maintains a temperature difference of 3-5 K. The transmitted light intensity was acquired with the aid of a PMT module

(H10721-110, made by Hamamatsu) and stored in a computer via Keithley 2000 multimeter. During heating/cooling cycle at a rate of 0.5 °C min^{-1}, the measured data points were acquired in a computer with a programmable software at an interval of 2 or 3 seconds which leads to a temperature difference of about 0.017 °C or 0.025 °C between successive data points respectively. Furthermore, another PMT module was used to detect the fraction of incident light obtained by a beam splitter in order to monitor the stability of incident LASER beam during the experiment. Fig. 2.3 represents the experimental set-up used to measure temperature variation of the high-resolution optical birefringence for the investigated LC samples.

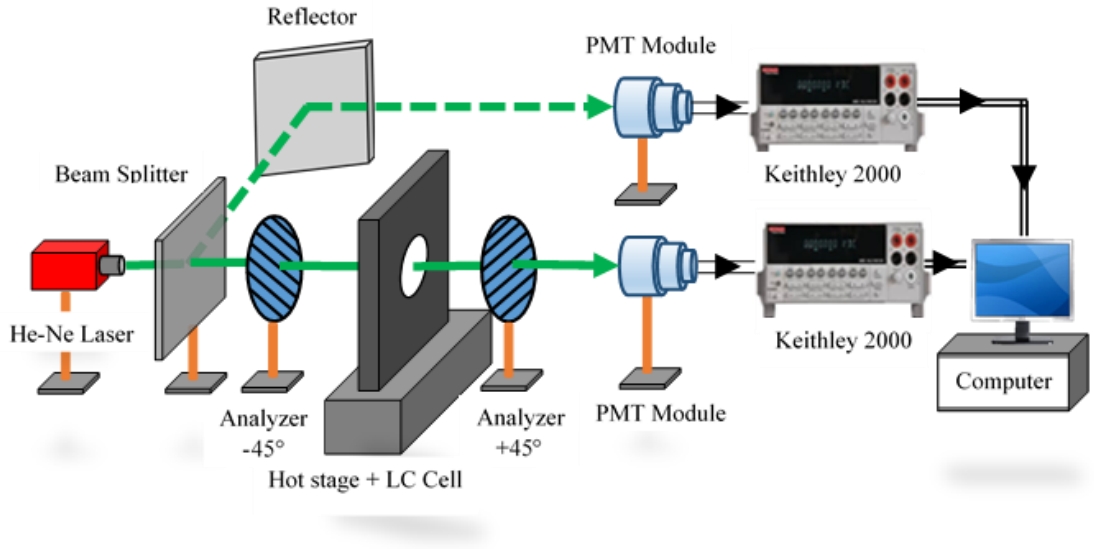

Figure 2.3. Schematic diagram of the experimental set-up for optical transmission measurement.

The normalized transmitted light intensity or transmittance of the LASER beam can be expressed in terms of phase retardation ($\Delta\varphi$) and can be written as [22]

$$I_t = \frac{\sin^2 2\theta}{2}(1 - \cos\Delta\varphi) \qquad (2.2)$$

where 2θ is the angle between the polarizer and analyzer and the corresponding phase retardation can be expressed as

$$\Delta\varphi = \frac{2\pi}{\lambda}\Delta n d \qquad (2.3)$$

where Δn is the optical birefringence of the studied liquid crystal sample, d is the LC cell thickness and λ is the corresponding wavelength of LASER beam. For a precise measurement, each one of the polarizer and analyzer was held at an angle of 45° in clockwise and anti-clockwise directions respectively with respect to optic axis which effectively produces a total angle (2θ) about 90° or $\pi/2$ between the analyzer and the polarizer. The oscillatory transmitted intensity of LASER beam possesses maxima and minima for $\Delta\varphi = (2m+1)\pi$ and $2m\pi$, where m is an integer. Therefore, the optical birefringence value can be evaluated from the analysis of transmitted intensity data and the associated value of the phase retardation [17-21, 23].

Experimental works under this dissertation have been performed for studied liquid crystal samples filled in commercially available indium tin oxide (ITO) coated glass cells for different thickness (5-9 μm) in planar as well as homeotropic alignments. As the liquid crystal samples gradually increase the molecular ordering from the isotropic state to lower temperature mesophases, all the experimental data for investigated compounds were taken during cooling cycle. The sensitivity in the measurement of Δn values was found to be better than 10^{-5} for the 5 μm thick sample.

2.2.5. Static dielectric permittivity measurement

The liquid crystal sample act as a dielectric material and possesses dielectric anisotropy, *i.e.*, the anisotropy is present in between parallel and perpendicular (with respect to the molecular long axis or the director **n**) component of the dielectric permittivity. This is due to the presence of one or more polar groups or atoms attached with the organic molecules produces a dipole moment. Investigation of temperature dependent permittivities gives an idea about the intermolecular dipole-dipole interaction and relative orientation of the molecules in different mesophases. Such information about the dielectric

parameters of LC samples at different mesophases endows us to use in different application purposes.

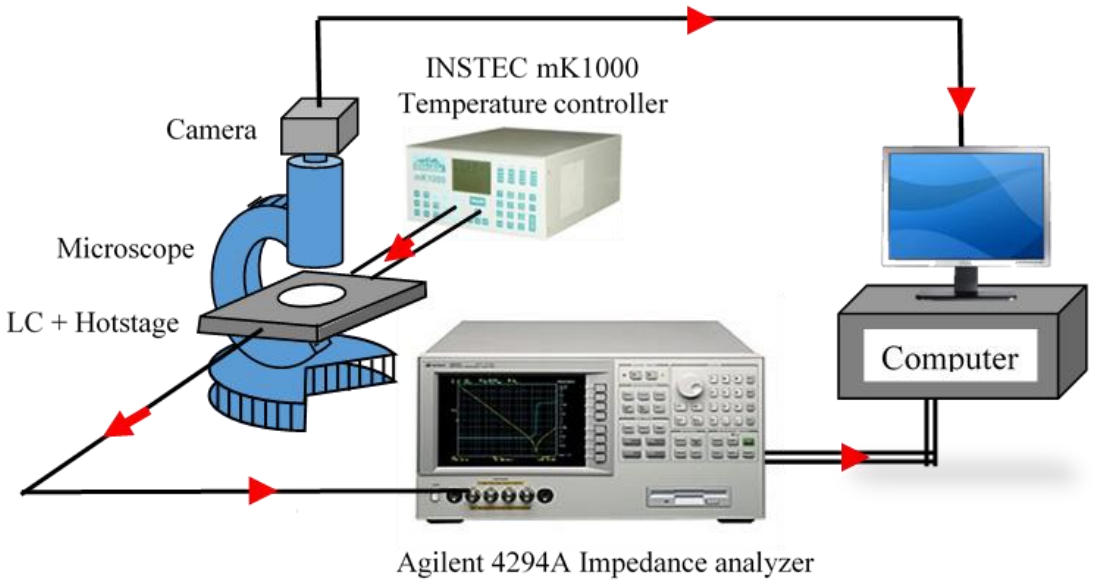

Figure 2.4. Schematic diagram of the experimental set-up for the dielectric study.

To obtain the temperature-dependent capacitance value, LC compounds were filled within the ITO coated cells in both planar and homeotropic alignments. The empty cell capacitance (C_0) was measured prior to filling with samples. The LC cells were placed in a hot/cool stage (HCS 302) made by INSTEC with the aid of a programmable temperature controller mK1000 (INSTEC) having a maximum temperature resolution of 0.001 °C. The temperature variation of capacitance value was measured by using Agilent 4294A precession impedance analyzer (40 Hz –110 MHz) with a relative accuracy of ±0.08%. Measured data points were collected in a computer suitably interfaced with the impedance analyzer [24-27]. The set-up for the measurement of dielectric study is shown in Fig. 2.4. Moreover, to determine the stray capacitance, the capacitance value of some standard materials was measured such as ultrapure water, pure benzene and *para*-xylene etc. If C_0 is the capacitance of the air-filled cell and C_a is that of the empty cell excluding the stray capacitance C_S, then it can be expressed as:

$$C_0 = C_a + C_s \quad (2.4)$$

Now, for a standard material of dielectric permittivityε, one can write it as:

$$C = \varepsilon C_a + C_s \quad (2.5)$$

where C presents the capacitance of the cell filled with the standard material. By solving the above equations it is possible to determine the related stray capacitance C_s and the dielectric permittivity of a fluid can be evaluated using the following relation:

$$\varepsilon = \frac{C - C_s}{C_0 - C_s} \quad (2.6)$$

The accuracy of the experimental setup had been validated by measuring the dielectric permittivities of the compounds 5CB and 7CB, which were found to be in close agreement with those reported in the literature [28].

In effect of applying an external voltage (fixed frequency), LC system consisting of polar molecules produces an orientational polarization in addition to their induced polarization. This orientational polarization along and perpendicular to the field direction is reflected by the measurement of dielectric permittivities. Therefore, the temperature dependent parallel ($\varepsilon_{\parallel}$) and perpendicular ($\varepsilon_{\perp}$) components of static dielectric permittivities for the investigated systems were determined throughout the entire mesomorphic range by using homeotropic and planar aligned cells respectively. Furthermore, the dielectric anisotropy $\Delta\varepsilon$ (= $\varepsilon_{\parallel}$-$\varepsilon_{\perp}$) and the average dielectric permittivity $\{\varepsilon_{avg} = 1/3(2\varepsilon_{\perp}+\varepsilon_{\parallel})\}$ values were calculated with the help of the obtained parallel and perpendicular permittivity values [24-27].

2.2.6. Dielectric spectroscopy measurement

The dielectric spectroscopy measurement has been carried out by the computer controlled Agilent 4294A impedance analyzer (40 Hz-110 MHz) in ITO coated LC cell of different thickness both in the planar and homeotropic orientations. The sample filled cells were placed within a programmable hot stage HCS302 (INSTEC), the temperature of which was controlled and

measured by mK1000 thermo system designed by INSTEC (Fig. 2.4). Investigation of the dielectric parameters and molecular relaxations has been performed in order to obtain the real and imaginary parts of the impedance in the frequency range 40 Hz to 15 MHz with a maximum AC applied voltage of 0.5 V (RMS) to avoid nonlinear responses. The measurement was carried out at a fixed temperature and recorded in each temperature starting from the isotropic phase to the entire mesomorphic range at an interval of 1 °C. The frequency dependent complex dielectric permittivity is given by $\varepsilon^*(f) = \varepsilon'(f) + i\varepsilon''(f)$, where $\varepsilon'(f)$ represents the real part of dielectric permittivity (representation spectrum is called the dispersion curve), and $\varepsilon''(f)$ stands for the imaginary part of the complex permittivity (representation spectrum is called the absorption curve). Firstly, the capacitance (C_p) and conductance (G) values (in a parallel equivalent circuit) were accumulated from the instrument and then the real (ε') and imaginary (ε'') parts of dielectric permittivity have been calculated from the measured C_p and G data points by using following relations [29,30]:

$$\varepsilon' = \frac{C_p - C_s}{C_0 - C_s} \tag{2.7}$$

$$\varepsilon'' = \frac{G}{2\pi f C_p} \tag{2.8}$$

where f is the frequency, C_0 is the empty cell capacitance and C_S is the stray capacitance. The variation of frequency dependent ε' and ε'' are displayed in Fig. 2.5 for an investigated sample.

In order to study the measured temperature dependence relaxation modes, $\varepsilon^*(f)$ has been compared with the Havriliak-Negami (H-N) function [31,32] with the addition of a conductivity contribution (3rd term) term present at lower frequencies, which is expressed as:

$$\varepsilon^*(f) = \varepsilon_\infty + \sum_{k=1}^{N} \frac{\Delta\varepsilon_k}{[1+(if\tau_k)^{\alpha_k}]^{\beta_k}} - \frac{i\sigma_0}{\varepsilon_0(2\pi f)^n} \tag{2.9}$$

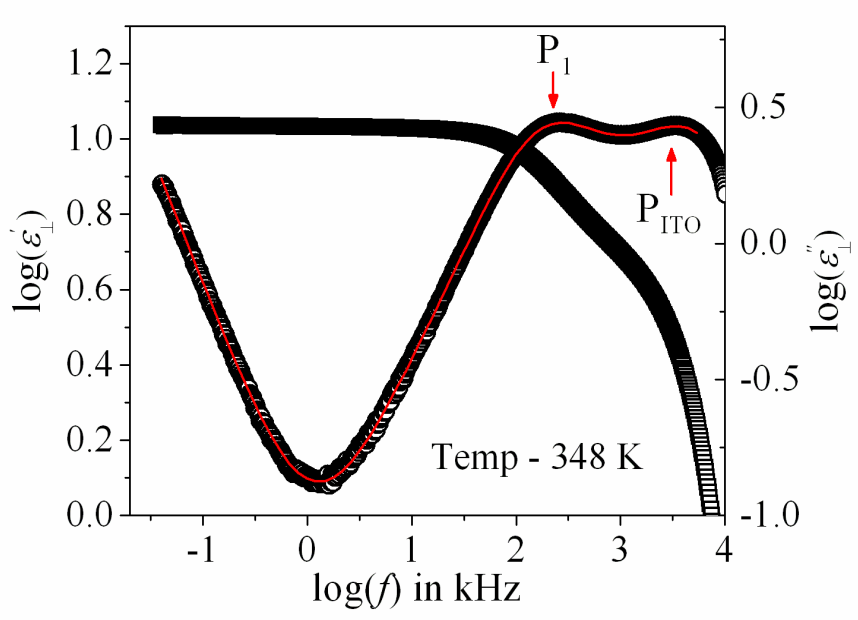

Figure 2.5. Frequency-dependent variation of the real (ε') and imaginary (ε'') parts of dielectric permittivity for a fixed temperature of a bent-core compound-**1/7** (described in chapter 8).

The real and imaginary parts of the complex dielectric permittivity were fitted with the Havriliak-Negami (H-N) fitting functions [33,34] given below:

$$\varepsilon' = \varepsilon_\infty + \sum_{k=1}^{N} \frac{\delta\varepsilon_k[1 + (2\pi f\tau_k)^{\alpha_k}\cos(\alpha_k\pi/2)]}{[1 + (2\pi f\tau_k)^{2\alpha_k} + 2(2\pi f\tau_k)^{\alpha_k}\cos(\alpha_k\pi/2)]} \tag{2.10}$$

$$\varepsilon'' = \frac{\sigma_0}{(2\pi f)^S} + \sum_{k=1}^{N} \frac{\delta\varepsilon_k[1 + (2\pi f\tau_k)^{\alpha_k}\sin(\alpha_k\pi/2)]}{[1 + (2\pi f\tau_k)^{2\alpha_k} + 2(2\pi f\tau_k)^{\alpha_k}\cos(\alpha_k\pi/2)]} \tag{2.11}$$

where $\delta\varepsilon_k$ is the dielectric strength, ε_∞ is the high-frequency limit of permittivity, τ_k ($=1/2\pi f_k$) is the relaxation time, f is the corresponding relaxation frequency, α_k and β_k are shape parameters describing the symmetric and non-symmetric broadness of the dielectric dispersion curve respectively, ranging between 0 and 1, and k is the number of relaxation processes. Here σ_0 is related to the DC conductivity and S is a fitting parameter responsible for the slope of the conductivity. Corresponding fitting lines are also included in the representative figure (Fig. 2.5).The H-N response reduces to Cole-Davidson [35] response when $\alpha = 1$ and to Cole-Cole [36] response when $\beta = 1$.

In addition to this, an external DC bias voltage was varied from 1 V to a maximum available 40 V to find the effect of applied voltage on the relaxation modes. The effect of bias voltage on the relaxation modes as well as on the optical textures at different mesophases has been studied in ITO coated cells placed between the two crossed polarizer of the optical microscope.

2.2.7. Splay elastic constant measurement

In case of uniaxial nematic phase, the molecular director is aligned on average in a particular direction which describes the entire phase alignment direction. However, the uniform nematic phase of the liquid crystal compounds can be deformed by applying external electric or magnetic field as well as by surface boundaries or particle inclusions. The free energy of this deformed state is evidently higher than that of the equilibrium state. Hence, due to the existence of such perturbed forces in the deformed state, some opposite elastic restoring torques of nematogens developed within the system those are always trying to restrict the deformation of the director field and known as restoring stresses [37]. In 1933, Oseen [38] and Zocher [39] proposed that such perturbations of molecular director (director curvature) can be well described by the elastic continuum theory which is analogous to the classical elastic theory of solids. Furthermore, in 1958, Frank [37] explored it again by presenting the theory of curvature elasticity. Basically, each of the deformation modes are described individually by an elastic constant [40-44] and expressed as follows: the splay (K_{11}), twist (K_{22}) and bend (K_{33}) elastic constants which are also known as the Frank elastic moduli. According to the elastic continuum theory [44], the elastic free energy of deformed nematic phase is given by:

$$F_{def} = \frac{1}{2}\left[K_{11}\left(\vec{\nabla}.\hat{n}\right)^2 + K_{22}\left(\hat{n}.\vec{\nabla}\times\hat{n}\right)^2 + K_{33}\left(\hat{n}\times\vec{\nabla}\times\hat{n}\right)^2\right] \qquad (2.12)$$

where K_{11}, K_{22} and K_{33} are the elastics constants known as Frank elastic constant whereas $\hat{n}$ is the nematic director.

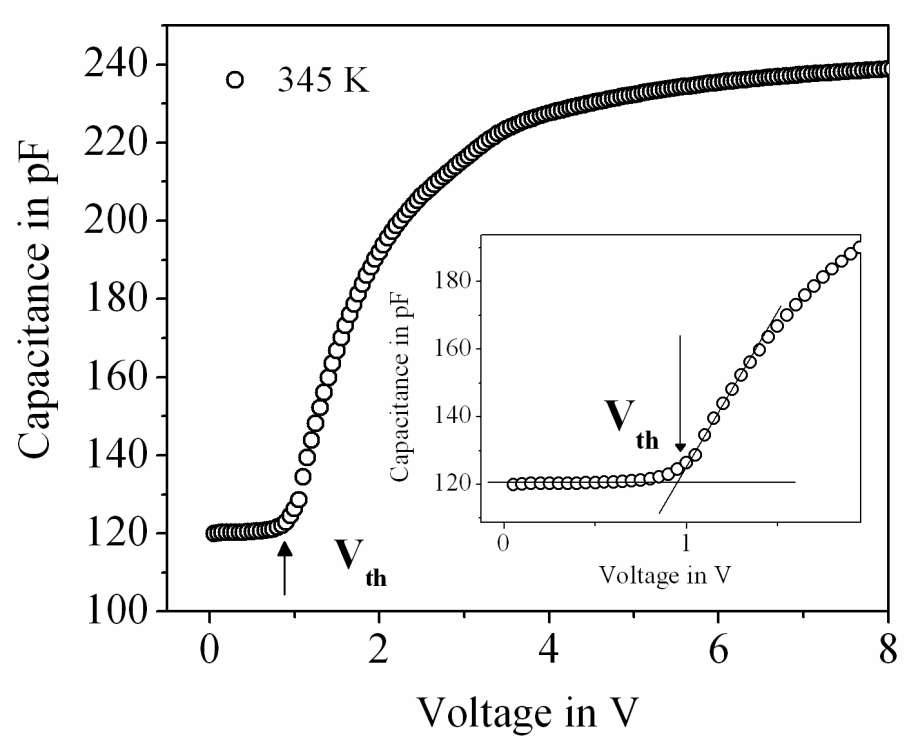

Figure 2.6. Voltage dependent variation of sample filled cell-capacitance due to electrically driven Freedericksz transition in the nematic phase of a binary mixture (described in chapter 4) at 345 K. Inset shows the closer view near the threshold voltage.

Out of them, this dissertation only deals with the measurement of splay elastic constant for the nematic liquid crystal sample by the method of field-induced Freedericksz transition [45-48]. Although the Freedericksz transition can be observed by an externally applied electric [49-51] or magnetic field [52-56], only the electric field has been applied in the experiments. Due to an application of sufficiently strong electric field to a planar aligned mesogenic medium in an orthogonal direction to the molecular long axis, the Freedericksz transition [49-51] develops within the system, resulting in a deformation of the molecular directors along the field direction. Beyond this Freedericksz threshold voltage (V_{th}), the capacitance value ($C_{\perp}$) for planar aligned sample sharply increases up to a saturation value ($C_{||}$) as shown in Fig. 2.6. However, these V_{th} and $C_{||}$ both depend upon the sample temperature.

Prior to determining the splay elastic constant (K_{11}), at first the threshold voltage was evaluated in planar aligned ITO coated LC cell of suitable thickness by applying a sinusoidal voltage whose amplitude is maximum up to 20 Volt at a fixed frequency of 1 kHz. The capacitance value (C) of the nematic liquid crystal was measured by the small variation of applied electric field voltage (V) by using Agilent E4980A precession LCR-bridge with an accuracy of $\pm$ 0.05% [49,57-59]. This process has been performed at a fixed temperature and recorded it in a computer in each temperature starting from the isotropic phase to the entire nematic phase at a small temperature interval. Fig. 2.6 represents a voltage-dependent capacitance curve at a fixed temperature for a LC sample in the nematic phase. During this experiment, the temperature was controlled and measured by a temperature controller Eurotherm PID 2404 with an accuracy level ±0.1 $^{\circ}$C. The temperature dependent values of threshold voltage V_{th} (value of applied voltage where the deformation starts) were calculated from this C-V curve and hence the splay elastic constant was determined by the following relation [60-62]:

$$K_{11} = \frac{\varepsilon_0 \Delta\varepsilon V_{th}^2}{\pi^2} \tag{2.13}$$

where $\Delta\varepsilon$ is the dielectric anisotropy value of that nematic LC sample and ε_o is the free space permittivity, while V_{th} is the threshold voltage in r.m.s.

2.2.8. Rotational viscosity measurement

The rotational viscosity (γ_1) of the nematic liquid crystal is the crucial parameter for the application purpose in display technology [63]. The rotational viscosity of the material defines the molecular dynamics of the molecules within the sample and it is correlated to the torque associated with the molecular rotation in response to an external perturbing field. Moreover, it is dependent upon the molecular structure and their association as well as the temperature of the compound. Due to the rotation of molecules, an internal

friction between the molecular directors is developed which is represented by the rotational viscosity of that material. Therefore, the higher value of rotational viscosity corresponds to a slower response to the external field and vice versa.

For the investigated LC systems, firstly the response time (τ_0) and consequently the rotational viscosity (γ_1) values were determined by capacitive relaxation method [25,58,64] with the aid of Agilent 4980A digital impedance analyzer. An external AC voltage (V) having a magnitude above the corresponding threshold voltage (V_{th}) at a frequency 10 kHz has been applied in the nematic phase. The investigated sample was mounted in a planar aligned ITO coated cell of suitable thickness. After a certain time interval (in second), when the external field was suddenly removed, the molecular directors start to reorient to the equilibrium state (or energy-minimized state) and the time taken by the molecules to be relax back was characterized by the relaxation time (τ_0) of the nematic LC sample at a particular temperature. Hence, a voltage-dependent value of capacitance was accumulated through the impedance analyzer and stored in a computer with the help of programmable software. This process was repeatedly done in a certain temperature interval starting from the isotropic phase over the entire nematic phase. For a particular temperature, the difference between the instantaneous capacitance (C_t) at a particular time t and the equilibrium state capacitance ($C_\perp$) (for homogeneous alignment) in a small signal regime execute [64] a simple exponential decay curve which can be expressed as:

$$\Delta C_t = C_t - C_\perp = \Delta C_0(exp(-2t/\tau_0)) \qquad (2.14)$$

where τ_0 is the relaxation time and $\Delta C_0 \approx C_\perp(\Delta\varepsilon/2\varepsilon_\perp)\varphi_m$ for planar alignment cell in which $\Delta\varepsilon$ is the dielectric anisotropy, $\varepsilon_\perp$ is the perpendicular component of the static dielectric permittivity, $C_\perp$ is the capacitance of the cell when the molecules are aligned orthogonal to the substrate and φ_m is the director tilt angle at the middle of the layer at time $t = 0$, *i.e.*, when the relaxation is being

initiated. Furthermore, several experimental results [64] reveal that Eq. (2.14) demonstrates a good approximation for $\varphi_m < 1$. Therefore, the relaxation time (τ_0) was measured from the slope of a logarithmic plot of the transient capacitance ($\Delta C_t/C_\perp$) as a function of time at a particular temperature and hence the required rotational viscosity for a planar aligned LC sample of thickness *d* can be calculated by using the following relation [25,58,60,64]:

$$\gamma_1 = \frac{\tau_0 K_{11} \pi^2}{d^2} \tag{2.15}$$

where K_{11} is the splay elastic constant for that compound. By varying the temperature at a certain interval, the temperature dependent rotational viscosity has been measured throughout in the entire nematic mesophase.

2.2.9. Electro-optical study

The electro-optical study for the investigated LC compounds was carried out by the field reversal polarization technique [65-68]. The LC materials were filled in planar aligned LC cells of a suitable thickness having an active area of about 0.25 cm^2 in between the ITO coated substrates. In this technique, an external electric field (square wave) having magnitude V_{pp} = 38 V at frequency, *f* = 20 Hz was applied to LC cells to drive a microscopic current through the material. For this purpose, a waveform generator Picotest G100A and the FLC (F20A) voltage amplifier (amplification factor 20 times) was used. The response current was measured from the value of voltage drop across the resistance connected in series to the sample filled cell as shown in Fig. 2.7. In some cases, triangular wave voltage has also been applied. Hence, an effective voltage ~ 8 Volt per μm acts on each cell and often higher voltage was applied to acquire the polarization effect in some LC samples. As the polarization was inverted by the input voltage, the polarization current pulse thus obtained and fed to a Digital Storage Oscilloscope (Agilent DSO X2000A). The input and output waveforms were obtained in a computer suitably interfaced with the oscilloscope. This polarization current pulse

represents a hump in the spectrum while a sharp peak was observed in case of a triangular wave input voltage. Fig. 2.8(a) and Fig. 2.8(b) represent the input and output waveforms for both the square and triangular waves respectively.

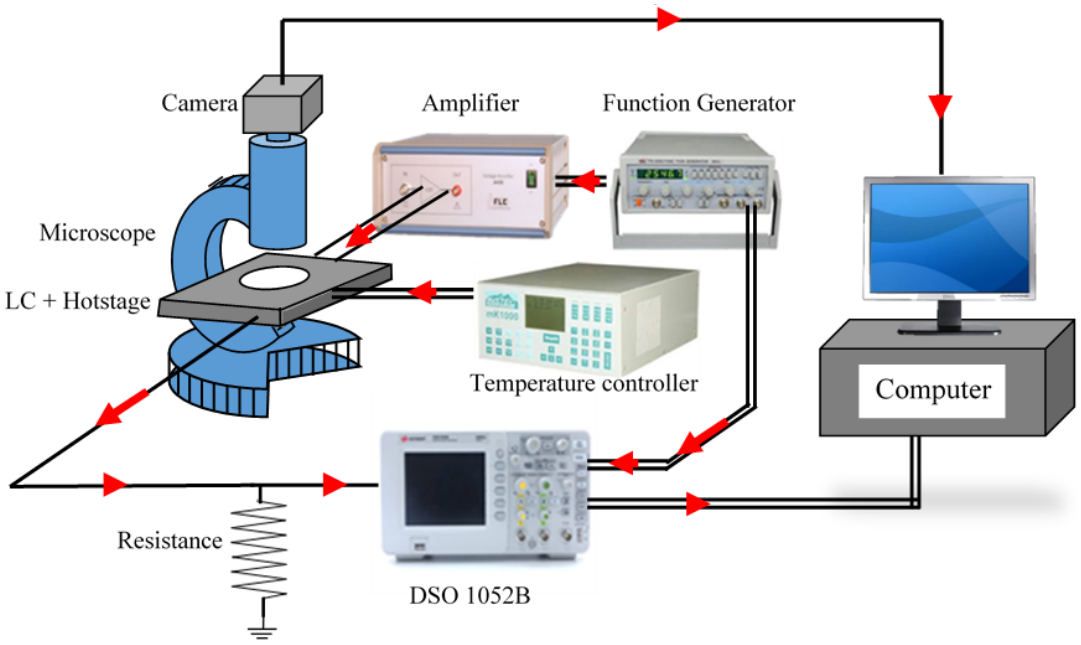

Figure 2.7. Schematic diagram of the experimental set-up for electro-optical study using field reversal polarization technique.

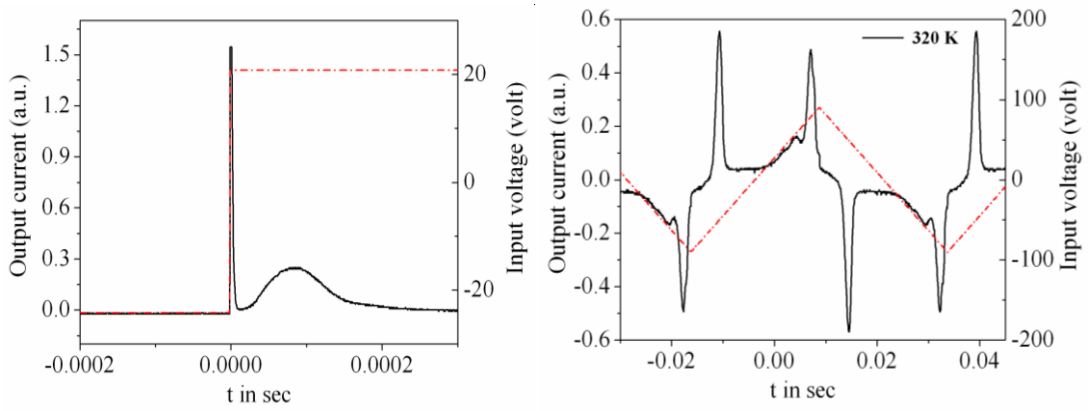

(a) (b)

Figure 2.8. Input and output waveforms of the LC sample for (a) square wave and (b) triangular wave input voltages.

Moreover, the LC cell was placed in a hot/cool stage HCS 302 designed by INSTEC, USA, equipped with a programmable temperature controller mK1000, by which temperature was varied at a rate of 0.5 K per minute.

Additionally, the optical textures were also observed at the ON and OFF state of the external field to detect the polarization effect visually.

The liquid crystal material sandwiched between two electrode surfaces can be regarded as a parallel combination of a capacitor (C) and a resistance (R). Hence, for the given circuit arrangement, a polarization current (I_P) is produced in the LC cell due to the reorientation of polarization ($\overrightarrow{P_S}$) for the reversal effect of the input voltage. In addition to this, there exist two more current components, the current I_C for the charge accumulation in LC cell capacitor and the current I_I is produced due to the ionic contribution of liquid crystal sample. Therefore, an effective current (I) pass through the LC cell [66] can be written as:

$$I = I_P + I_C + I_I = \frac{dP}{dt} + C\frac{dV}{dt} + \frac{V}{R} \tag{2.16}$$

where P represents the induced charge due to the polarization realignment, *i.e.*, the amount of induced charge at the time of sign reversal of spontaneous polarization (P_s) in accordance with the input voltage. R is the effective resistance in the circuit where V is the voltage of input signal. In order to determine the polarization current (I_P), neglecting the other contributions in output current, a proper baseline correction has to be performed by using mathematical software. However, the spontaneous polarization values were evaluated by integrating the hump/peak area (A) of the output current spectrum by the following expression [68]:

$$P_s = \frac{1}{2A}\int I dt \tag{2.17}$$

In this study, the values of the spontaneous polarization have been measured with a precision of ± 0.9 nC/cm^2.

Additionally, the relaxation time or response time (τ) has also been obtained by measuring the time taken by the output current to fall or rise from 10% to 90% of the peak value in response to the square wave input signal [69] and it can be expressed as [68,69]:

$$\tau = \frac{t_{10-90}}{1.8} \tag{2.18}$$

The effective torsional bulk viscosity (η) was obtained using the following relation:

$$\eta = P_s E \tau \tag{2.19}$$

where E is the externally applied electric field. In this study, the free relaxation time and the effective torsional bulk viscosity were determined within an accuracy of ± 1 μs and ± 0.9 Pa s respectively.

2.3. Theoretical background

2.3.1. Maier-Saupe Theory

There are several fundamental theories regarding the liquid crystal mesophases and associated phenomenological theories related to different mesophase transitions. Among them, the molecular mean-field approximation is the simplest theoretical approach to describe the thermodynamical behavior of the nematic phase as well as the qualitative discussion about the isotropic-nematic phase transition. According to mean field theory, molecules are assumed to be rod-like and possess cylindrical symmetry with a tendency to align their long axes in a particular direction (director, $\hat{n}$). Again, a molecule orients under the action of a mean field due to interactions with the other molecules of the system. Maier-Saupe [70-72] proposed the most successful microscopic theory to explain the statistical behavior of the molecules in the nematic phase (many particle systems) by assuming some approximations as follows:

(i) An attractive interaction between the adjacent molecules acts in the nematic phase.

(ii) The anisotropic part of the dispersion interaction energy between the molecules is responsible for the nematic molecular ordering within the system.

(iii) Due to the presence of long-range nematic orientational ordering, LC molecules are assumed to be neutrally charged and thus the influence of

permanent dipoles can be totally ignored.

(iv) The effect of induced dipole-dipole interaction should be considered for sustaining the nematic phase. However, the momentary dipole moment of one molecule induces the same to another molecule which results in an attractive interaction between them.

(v) The LC molecules are supposed to be considered as cylindrically symmetric along the long axis and the mutual interaction between any two adjacent molecules depends upon their relative angle.

(vi) The distribution of the molecular center of mass for the adjacent molecules is spherically symmetric with respect to a particular molecule.

In case of nematic liquid crystal system, Maier and Saupe proposed the concept of orientational ordering for the constituent molecules. Here the molecules are averagely aligned towards a particular direction, but due to the presence of external mean field the molecular long axes are distributed with respect to the director ($\hat{n}$) as a function of the angle (θ) between them. Thus each of the molecules are considered to experience an average attractive potential $V(\cos\theta)$ which can be expressed as:

$$V(\cos\theta) = \sum_{L-even} U_L \langle P_L \rangle P_L(\cos\theta) \qquad (L \neq 0) \tag{2.20}$$

where U_L is the function depends on the least distance between the central molecule and its adjacent neighbors only. $\langle P_L \rangle$ are termed as the orientational order parameters. $P_L(\cos\theta)$ is the L^{th} even order Legendre polynomial and the statistical average of $P_L(\cos\theta)$ is given by

$$\langle P_L(\cos\theta) \rangle = \int_0^1 P_L(\cos\theta) f(\cos\theta) d(\cos\theta) \tag{2.21}$$

However, the orientational distribution function $f(\cos\theta)$ in the nematic phase may be written as:

$$f(\cos\theta) = \sum_{L-even} \frac{(2L+1)}{2} \langle P_L(\cos\theta) \rangle P_L(\cos\theta) \tag{2.22}$$

Here the molecules in the nematic phase posses the head-tail symmetry, thus $f(\cos\theta)$ is an even function of $\cos\theta$. Again, by assuming L = 2, Eq. (2.21) modified as:

$$\langle P_2(\cos\theta)\rangle = \int_0^1 P_2(\cos\theta) f(\cos\theta) d(\cos\theta) \tag{2.23}$$

Generally, this $\langle P_2 \rangle$ is known as the order parameter for the liquid crystal system. The value of $\langle P_2 \rangle$ is considered as zero for an isotropic liquid while $\langle P_2 \rangle = 1$ for a perfectly ordered state or in crystal phase.

Consequently, the potential energy for a single molecule can be written by modifying Eq. (2.20) as follows:

$$V(\cos\theta) = -\nu P_2(\cos\theta)\langle P_2\rangle \tag{2.24}$$

where $\nu = -U_2$. However, the single-molecule orientational distribution function takes the form

$$f(\cos\theta) = Z^{-1}\exp[-V(\cos\theta)/kT] \tag{2.25}$$

where k is the Boltzmann's constant and Z serves to normalize the function $f(\cos\theta)$ which is the single molecule partition function that can be expressed as

$$Z = \int_0^1 \exp[-V(\cos\theta)/kT]\, d(\cos\theta) \tag{2.26}$$

Substituting all the values in Eq. (2.23), one can write

$$\langle P_2(\cos\theta)\rangle = \frac{\int_0^1 P_2(\cos\theta)\exp[P_2(\cos\theta)\langle P_2\rangle/T^*]d(\cos\theta)}{\int_0^1 \exp[P_2(\cos\theta)\langle P_2\rangle/T^*]d(\cos\theta)} \tag{2.27}$$

where, $T^* = kT/\nu$.

This is a self-consistent equation as it consists the term $\langle P_2 \rangle$ on both sides of the equation and the solution of it can be easily obtained by an iterative method in which one can get a temperature (T^*) dependent specific value of $\langle P_2 \rangle$ or of the order parameter. Now, in this case, one solution appears as $\langle P_2 \rangle = 0$ for all the temperatures in the isotropic or completely disordered phase.

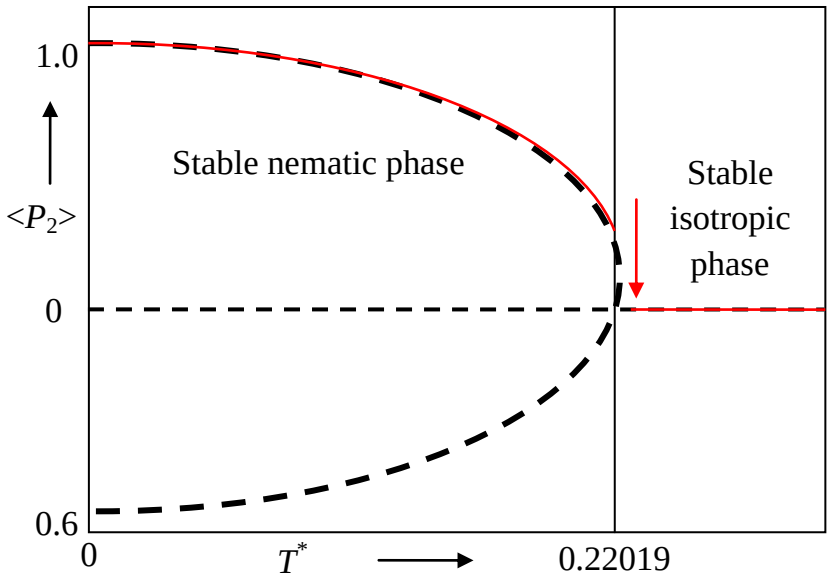

Figure 2.9. Orientational order parameter predicted from Maier-Saupe mean field theory.

Besides, two more solutions can be found for the temperatures $T^* < 0.22284$, as observed in Fig. 2.9. Eventually, a stable nematic phase exist with $\langle P_2 \rangle$ greater than zero for a condition $0 \leq T^* \leq 0.22019$ and for rest of the temperature range $T^* > 0.22019$, it reveals a thermodynamically stable isotropic phase having $\langle P_2 \rangle = 0$. However, by increasing temperature, the value of the order parameter $\langle P_2 \rangle$ decreases from unity (for completely ordered phase) to a minimum value about 0.4289 at $T^* = 0.22019$. Therefore, the pronounced *I–N* phase transition occurs at that temperature following a discontinuous change of $\langle P_2 \rangle$ from 0.4289 to 0 which reveals a first-order nature of the *I–N* phase transition. On the contrary, this transition is quite different than the solid to liquid first-order transition from the perspective issue of entropy change. The amount of entropy change is about 25 cal K^{-1} $mole^{-1}$ for usual solid-liquid transition while it is about 0.83 cal K^{-1} $mole^{-1}$ for the *I–N* phase transition which often known as weakly first-order transition. In several nematic LC compounds, the experimental data points of temperature dependent $\langle P_2 \rangle$ represents a close

agreement with the $<P_2>$ values obtained by solving self-consistent equation iteratively [43,73,74].

2.3.2. McMillan theory for the Sm-*A* phase

In order to characterize the macroscopical view-point of the Sm-*A* mesophase and also to reveal a satisfactory explanation about the *N*–Sm-*A* phase transition, McMillan [75,76] and Kobayashi [77-79] somewhat extended the mean field theory by considering an additional order character in the Sm-*A* phase. In general, the molecules in Sm-*A* phase possesses a one-dimensional positional ordering in addition to long-range orientational ordering of the nematic phase, *i.e.*, a periodic mass-density wave is present along the normal direction of smectic layers. Therefore, in order to sustain both the properties (parallel orientation of the molecular long axis along the director and the layer formation perpendicular to the director), a positional order parameter term is introduced in the expression of mean field potential energy function to describe the one-dimensional translational periodicity of the layered structure [75,76]. The effect of layering eventually leads to an enhancement of the orientational order parameter in the smectic phase relative to the nematic phase. However, in the Sm-*A* phase, the complete set of order parameters may be obtained by expanding the distribution function of a single molecule which depends on both spatial and angular coordinates. Hence, according to McMillan theory, the single molecule normalized distribution function for the Sm-*A* phase can be written as:

$$f(\cos\theta, z) = \sum_{L-even} \sum_n A_{L,n} P_L(\cos\theta) \cos\left(\frac{2\pi n z}{d}\right) \qquad (2.28)$$

where *d* is the layer thickness and the expansion coefficients those are related to the Sm-*A* phase order parameters [80] can be expressed as:

$$A_{L,n} = \{(2L+1)/d\} \langle P_L(\cos\theta) \cos(\tfrac{2\pi n z}{d}) \rangle \quad \text{L} \neq 0, \text{n} \neq 0 \qquad (2.29)$$

and the normalization condition is given by

$$\int_{-1}^{1}\int_{0}^{d} f(\cos\theta\,, z)\, dz\, d(\cos\theta) = 1 \qquad (2.30)$$

Following Kobayashi [77-79], McMillan [75,76] has considered an anisotropic term in pair interaction energy function. Therefore, by averaging the pair interaction potential for a single molecule over the second molecule it can be written as:

$$V_M(\cos\theta\,, z) = \langle U(r)\rangle + \langle W(r)\, P_2(\cos\theta)\rangle\; P_2(\cos\theta) \qquad (2.31)$$

where < *U(r)* > and < *W(r)* P_2 (cos θ) > are the functions of *z*, the spatial coordinates of the molecular center of mass with respect to smectic layer, while <….> denotes the statistical average of the quantities inside. θ is the angle between the molecular long axis with respect to the director.

By expanding it in Fourier series and taking the suitable averages, the potential function becomes

$$V_M(\cos\theta\,, z) = U_0 + U_1\tau\cos\left(\frac{2\pi z}{d}\right) + \ldots\ldots + [W_0\eta + W_1\sigma\cos\left(\frac{2\pi z}{d}\right) + \ldots\ldots]P_2(\cos\theta) \qquad (2.32)$$

where U_0, U_1, W_0, W_1 are the Fourier coefficients and η, τ and σ are the leading order parameters those can be represented as :

$$\text{Orientational order parameter: } \eta = \langle P_2(\cos\theta)\rangle \qquad (2.33)$$

$$\text{Translational order parameter: } \tau = \langle\cos(2\pi z/d)\rangle \qquad (2.34)$$

$$\text{Mixed order parameter: } \sigma = \langle P_2(\cos\theta)\cos(2\pi z/d)\rangle \qquad (2.35)$$

Moreover, due to the existence of short-range force, McMillan has considered the coefficients as $W_0 = -v$, $W_1 = -v\alpha$ and $U_1 = \delta W_1 = -\delta v\alpha$ where α and δ are the pair potential parameters. α is related to the length of the molecules and δ is associated with the ratio of the translational part of the potential to the orientational part of the same.

Consequently, the expression for effective pair potential of a single molecule in the Sm-*A* phase assumes the form

$$V_M(\cos\theta, z) = -v\left[\delta\alpha\tau\cos\left(\frac{2\pi z}{d}\right) + \left\{\eta + \alpha\sigma\cos\left(\frac{2\pi z}{d}\right)\right\} P_2(\cos\theta)\right] \quad (2.36)$$

Again, the distribution function for a single molecule can be expressed in terms of potential energy as follows:

$$f_M(\cos\theta, z) = Z^{-1}\exp[-V_M(\cos\theta, z)/kT] \quad (2.37)$$

where Z is the normalized partition function and can be written as:

$$Z = \int_0^1 \int_0^{\mathrm{d}} \exp[-V_M(\cos\theta, z)/kT]\, d(\cos\theta)dz \quad (2.38)$$

Therefore, the self-consistency equations for the above-mentioned order parameters appear as:

$$\eta = \int_0^1 \int_0^d P_2(\cos\theta) f_M(\cos\theta, z)\, d(\cos\theta)dz \quad (2.39)$$

$$\tau = \int_0^1 \int_0^d \cos(2\pi z/d)\, f_M(\cos\theta, z)\, d(\cos\theta)dz \quad (2.40)$$

$$\sigma = \int_0^1 \int_0^d P_2(\cos\theta)\cos(2\pi z/d)\, f_M(\cos\theta, z)\, d(\cos\theta)dz \quad (2.41)$$

Depending on the values of different potential parameters, the following three cases can be obtained:

i) when $\eta = \tau = \sigma = 0$, corresponds to the isotropic or completely disordered phase;

ii) when $\eta \neq 0$, $\tau = \sigma = 0$, corresponds to the nematic phase where only orientational ordering is present.

iii) when $\eta \neq 0$, $\tau \neq 0$, $\sigma \neq 0$, corresponds to smectic-*A* phase where both orientational and translational ordering is present.

All such significant solutions are obtained by solving the self-consistent Eqs. (2.39–2.41) by iteration method at several sets of values for α and δ. The major success of the McMillan theory is based on the prediction of the order nature of the nematic–smectic-*A* phase transition over the value of α and δ. If the value of $\alpha > 0.98$, there exhibit a direct transition from smectic-*A* to isotropic phase without stable nematic phase at any temperature. On the other

hand for $\alpha < 0.98$, it reveals two phase transition namely the isotropic–nematic (*I*–*N*) phase transition followed by the nematic–smectic-*A* (*N*–Sm-*A*) phase transition at comparatively low temperature. Although, McMillan theory divulges the *I*–*N* phase transition is of first order in nature, but the *N*–Sm-*A* transition can be either first order or second order depending on the value of α and a ratio (McMillan ratio) of the nematic–smectic-*A* and the isotropic–nematic phase transition temperatures respectively, *i.e.*, T_{NA}/T_{IN}. When $\alpha < 0.7$ and $T_{NA}/T_{IN} < 0.87$, it demonstrates a second order nature of the nematic–smectic-*A* (*N*–Sm-*A*) phase transition, whereas the value of T_{NA}/T_{IN} beyond 0.87, the *N*–Sm-*A* phase transition envisages a first-order transition in nature. Hence, this particular limiting point ($\alpha = 0.7$ and $T_{NA}/T_{IN} = 0.87$) where the *N*–Sm-*A* phase transition transforms its nature from second order to first order is referred to a tricritical point (TCP).

2.3.3. Landau-de Gennes theory for the *I*–*N* and *N*–Sm-*A* phase transitions

In LC system, Landau-de Gennes theory [80] is another qualitative endeavor as like mean-field theory which provides the semi-quantitative description about the isotropic–nematic transition. According to Landau, the free energy of the system is simply an analytic function of the order parameter and it is dependent upon the spatial derivatives at least near a second order phase transition [81,82]. To demonstrate a satisfactory explanation of the phase transitional phenomena in a macroscopic region, an extension of the Landau phenomenological theory [81,82] has been modified further by de Gennes [83], and again a brief review was given by Sheng and Priestly [84]. Thus, the Landau-de Gennes theory is a macroscopic manifestation of classical field theory, where the free energy function of the system can be expressed in terms of the order parameter in a power series in close vicinity to the transition. However, the order parameter is correlated with the symmetry of the thermodynamic system and further, a breaking of symmetry is associated with

a phase transition. Therefore, the order parameter of any thermodynamical system gathers the information about the change of symmetry as well as the change in different physical quantities in the neighborhood of phase transition.

According to Landau theory, the free energy density *f* (function of temperature *T*, pressure *P*, and order parameter *S*) in the absence of any external field can be expanded in power series with a lower ordered polynomial in terms of scalar order parameter *S* and generally expressed as:

$$f(T,S) = f(T,0) + \alpha S + \frac{1}{2}(AS^2) + \frac{1}{3}(BS^3) + \frac{1}{4}(CS^4) + \cdots. \quad (2.42)$$

where α, *A*, *B*, *C*,… are the phenomenological coefficients as well as a function of temperature and pressure but having no inherent physical significance. The free energy density in the most disordered phase is denoted by *f*(*T*,0).

In order to characterize the order parameter *S* of a system at a certain temperature *T*, the minimization condition $\left(\frac{df}{dS}\right) = 0$ is imposed on the free energy density function *f*, which results $\alpha = 0$ and $\frac{d^2f}{dS^2} = A$ for the disordered phase, *i.e.*, $S = 0$. Again from the symmetry consideration, the system has the reflection symmetry about *xy*-plane, which remains unchanged the free energy function for changing $S(\hat{z}) \rightarrow S(-\hat{z})$, *i.e.*, *f*(*S*) = *f*(-*S*). Therefore, the free energy function takes the form as an even function of the order parameter *S* leading to vanish the odd terms in the power series and hence $B = 0$, $D = 0$ etc. Thus, the remaining free energy density expression becomes

$$f(T,S) = f(T,0) + \frac{1}{2}(AS^2) + \frac{1}{4}(CS^4) + \cdots. \quad (2.43)$$

However, the coefficients were previously assumed as phenomenological, but it is still undefined about their dependency on the temperature. For this reason, all the coefficients can be expressed in power series with respect to the transition temperature T_C.

$$A(T) = a_0 + a'(T - T_C) + \ldots. ,$$

$$C(T) = c_0 + c'(T - T_C) + \ldots \quad \text{and so on.}$$

In this context, Landau has assumed that very close to the transition temperature ($T \approx T_C$), $a_0 = 0$ which again yields $A(T) = a'(T - T_C)$. Likewise, the second coefficient, the linear term can be neglected near the transition temperature which gives $C(T) = c_0$.

Now substituting all these values in Eq. (2.54), one can write:

$$f(T,S) = f(T,0) + \frac{1}{2}a'(T - T_C)S^2 + \frac{1}{4}c_0S^4 + \cdots \tag{2.44}$$

Furthermore, to determine the equilibrium value of *S*, the minimization condition is applied on the effective free energy density expression which gives $a'(T - T_C)S + c_0S^3 = 0$, and consequently the effective outcomes are represented as:

(i) One real solution, $S = 0$, for $T \geq T_C$ indicates a disordered phase.

(ii) Three other real solutions $S = 0, \pm\left(\frac{a'(T_C - T)}{c_0}\right)^{1/2}$, for $T < T_C$ in which first one ($S = 0$) depicts a local maxima and the other two symbolizes the positive and negative minima in free energy density curve as a function of order parameter *S*.

These solutions signify that the behavior of the order parameter *S* follows a scaling relation in the vicinity of transition point which can be expressed as:

$$S \propto (T_C - T)^{\beta} \tag{2.45}$$

where β is the order parameter critical exponent which gives a value 1/2 in mean field theory for Ising model, while in more precise theoretical and experimental reviews demonstrated a value 1/8 for 2D Ising model and ≈ 0.31 for 3D Ising system.

Furthermore, the phenomenological Landau theory, discussed in the previous section has been extended by de Gennes [83] to elucidate the first order mesophase transition exhibited by nematogens by including two basic

assumptions [85] – (i) The free energy density expansion (Eq. (2.42)) must contain up to sixth order term in which the coefficient of the third order term *B* assumes a value equal to zero, while $C < 0$ and the coefficient of the sixth term $E > 0$ is required to preserve the stability of the ordered phase. (ii) On the other hand, the third order term BS^3 is required in the free energy expansion as it is a tensorial quantity. Therefore, a first order mesophase transition can be obtained for a condition $B \neq 0$. The *I–N* phase transition defined so far in Landau theory as a second order nature because the molecules do not reveal any ordering in the isotropic phase and exhibit a continuous change in the order parameter value at the transition point [80,83-88]. Nevertheless, close investigation near the transition point suggests that the molecules are locally oriented in parallel to each other, results in a local molecular order which persists over a finite extent. de Gennes [83] named it as coherence length, which is dependent upon the temperature. Using this conceptual frame of reference and other thermodynamical assumptions, de Gennes [83] first successfully employed the power expansion series of the order parameter in a tensorial form in order to explain the first order nature of the isotropic-nematic (*I–N*) phase transition in liquid crystal systems. Generally, the nematogens are portrayed by an order parameter in the form of a traceless symmetric tensor, called the order tensor (*X*) *i.e.*, $X_{ii} = 0$ [43]. Now, in this case, the free energy density can be expressed in a power series in terms of tensorial order parameter *X* as follows:

$$f_n = f_i + \frac{1}{2}A\left(X_{ij}X_{ji}\right) - \frac{1}{3}B\left(X_{ij}X_{jk}X_{ki}\right) + \frac{1}{4}C\left(X_{ij}X_{ji}\right)^2 \qquad (2.46)$$

where f_i and f_n represents the Helmholtz's free energy at the isotropic and nematic phases respectively and *A, B, C* are the free energy coefficients in the form of a tensor. Now being a scalar, the Helmholtz's free energy expansion in powers of *X* containing only the terms those have invariant combinations of X_{ij} of the order parameter [86]. However, the negative sign of *B* is chosen for convenience.

Now this free energy expansion emerges a mesophase transition near the transition point if the coefficient *A* vanishes, *i.e.*, *A* = 0, but has no dependency on *B* and *C*. Thus it can be concluded that this phase transition is always driven by the influence of the coefficient *A* and assumed to take a form as $A = A'(T - T^*)$. Here T^* is the super-cooling temperature which is close to the *I–N* transition temperature while *B* and *C* are taken to be constant. Furthermore, for a uniaxial liquid crystal system, X_{ij} can be written as $X_{ij} = 1/2[S(3n_i n_j - \delta_{ij})]$, where *S* is the scalar order parameter and δ_{ij} is the identity tensor. Substituting all these values into Eq. (2.46), the free energy density assumes a form:

$$f_n = f_i + \frac{1}{3}A'(T - T^*)S^2 - \frac{2}{27}BS^3 + \frac{1}{9}CS^4 \qquad (2.47)$$

In order to determine the value of order parameter in an equilibrium state, minimization condition is applied on the effective free energy density expression which provides the equilibrium order parameter values as follows:

(i) *S* = 0, for the isotropic phase, and

(ii) $S_{\pm} = \left(\frac{B}{4C}\right)[1 \pm \{1 - 24\beta(T - T^*)\}^{1/2}]$ for the nematic phase (2.48)

where $\beta = A'C/B^2$. However, at the *I–N* phase transition temperature (T_{IN}) the free energy density must be equal in both sides. Hence, the desired transition temperature obtained from Eq. (2.47) and (2.48) can be written as:

$$T_{IN} = T^* + 1/27(B^2/A'C) \quad \text{for } \beta = 1/27 \qquad (2.49)$$

and the corresponding value of order parameter also can be represented by $S_{IN} = \frac{B}{3C}$ at that temperature which depicts a stable nematic phase. On the other hand if $T_{IN} = T^*$, the order parameter value drops at $S_{IN} = 0$ which represents the stable isotropic phase. From Eq. (2.49), it is observed that the temperature T^* is slightly lower than T_{IN}, where the isotropic phase is comparatively unstable. Similarly, there is an upper limit of T_{IN} where the nematic phase becomes unstable and it is possible when β = 1/24. This limiting

concept approaches another temperature $T^{**} = T_{IN} + 1/24(B^2/A'C)$ which is the maximum temperature limit of the stable nematic phase during the heating cycle. The cubic term in the free energy density expression describes the first order mesophase transition. However, for B tends to zero, T_{IN} defines the second order phase transition at temperature T^*. The temperatures T^* and T^{**} also have the significance that they are the apparent "critical points" for the isotropic and orientationally ordered nematic phases respectively. T^* and T^{**} are also known as the spinodal temperatures. Therefore, four different temperature regions are observed in this situation- (i) $T > T^{**}$, stable isotropic phase with $S = 0$, (ii) $T_{IN} < T < T^{**}$ corresponds to metastable nematic phase during heating, (iii) $T^* < T < T_{IN}$, represents a nematic phase and a possibility to occur super-cooled isotropic phase, (iv) $T < T^*$, signifies a thermodynamically stable nematic phase. An analogical representation of order parameter (S) with the variation of temperature (T) for a first-order isotropic–nematic phase transition is shown in Fig. 2.10(b). However, the order parameter value approaches to zero at the isotropic–nematic (I–N) phase transition temperature (T_{IN}).

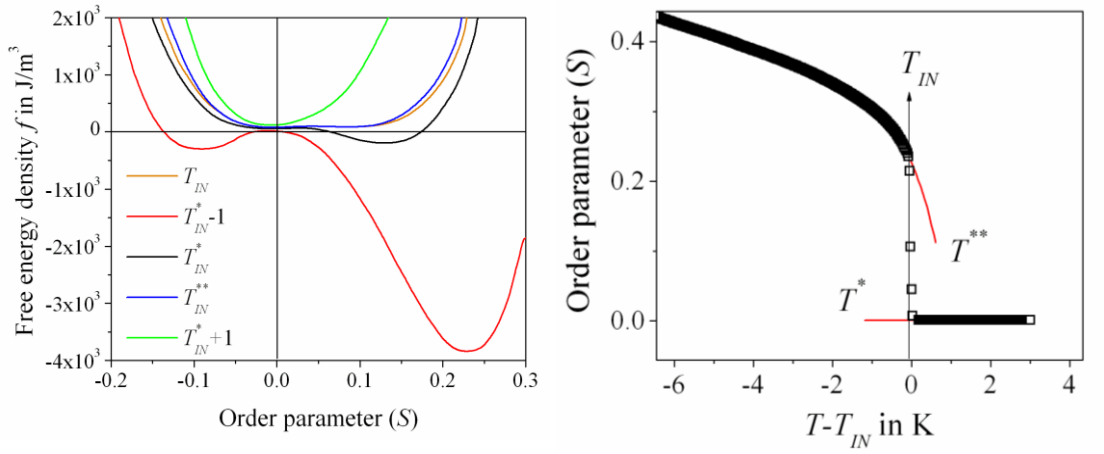

(a) (b)

Figure 2.10. (a) The free energy density (f) as a function of scalar order parameter S. (b) The nematic order parameter (S) vs. temperature. T^* and T^{**} are the temperatures slightly lower and higher than T_{IN} respectively.

Furthermore, Landau-de Gennes theory of the isotropic–nematic (*I–N*) phase transition has also been extended to the nematic–smectic-*A* (*N*–Sm-*A*) phase transition by considering an additional order parameter term of the Sm-*A* phase in the free energy expansion. As the Sm-*A* phase has a translational ordering in addition to orientational ordering of the LC molecules, they are supposed to be aligned perpendicularly within the equidistant layers. Hence, the Sm-*A* phase is characterized by an effective one-dimensional periodic density wave along the perpendicular direction ($\hat{z}$) with respect to the layer plane [75,87] and can be expressed as

$$\rho(r) = \rho(z) = \rho_0 + \sum_{i=1}^{\infty} \rho_i \cos\,(iq_s z - \varphi_i) \qquad (2.50)$$

while in case of nematic phase the fundamental term ρ_1 becomes zero but it provides a significant value for smectic-*A* phase and φ_i is the arbitrary angle of the molecules with respect to the director. However, the free energy density expansion in the *N*–Sm-*A* phase transition contains only even power terms as because the density wave function is invariant under translation, *i.e.*, (Ψ) = -(Ψ). Hence, the free energy expansion at the *N*–Sm-*A* phase transition is expressed as

$$\Delta f_1 = \frac{1}{2} r\rho_1^2 + u_0\rho_1^4 + \ldots\ldots \qquad (2.51)$$

Here the coefficient r is assumed as $r = \alpha(T - T_0)$, where T_0 is the closest temperature to the *N*–Sm-*A* phase transition temperature (T_{NA}). In this context when u_0 is greater than zero and also $T > T_0$, the value of r leads to a positive value and when $T < T_0$, the value of r is seen as negative. By considering the above conditions, the *N*–Sm-*A* phase transition reveals a second order transition at the mean field temperature $T_0 = T_{NA}$. However, the situation became more complicated when the coupling with the nematic order parameter $S_0 = \frac{1}{2}\langle 3cos^2\theta - 1\rangle$ has been taken into account. Again, if a small deviation ($\delta S = S\text{-}S_0$) of the nematic order parameter occurs at the transition, the free energy density expansion becomes:

$$\Delta f_2 = \frac{1}{2} r\rho_1^2 + u_0\rho_1^4 + \frac{1}{2\chi}\delta S^2 - C\rho_1^2\delta S \qquad (2.52)$$

where χ is the response function (susceptibility) which assumes a smaller value at the *N*–Sm-*A* phase transition and provides a greater value at the *I*–*N* phase transition and *C* is a positive constant. Moreover, by imposing the minimization condition on free energy density expansion, it gives:

$$\delta S = \chi C\rho_1^2 \qquad (2.53)$$

with
$$u = u_0 - 2C^2\chi \qquad (2.54)$$

So *u* is dependent on the values of χ and *C*. The sign convention of the quantity *u* reveals the order nature of the *N*–Sm-*A* phase transition. If χ approaches a smaller value then *u* gives a positive sign which yields a second order nature of the *N*–Sm-*A* phase transition at $T_0 = T_{NA}$, while *u* is negative for a higher value of χ, it divulges a first-order transition at $T_{NA} > T_0$ provided for a free energy expansion up to sixth order term. Furthermore, at $u = 0$, $\chi = \frac{u_0}{2C^2}$; it ensures a crossover from second order transition to first order transition through a tricritical point [TCP] on the *N*–Sm-*A* transition line. Although a stronger coupling acts between the nematic and Smectic-*A* order parameters which drives the transition from second order nature to the tricritical region [88], McMillan has considered this occurrence of tricritical point for a value of McMillan ratio (T_{NA}/T_{IN}) equal to 0.87 which is somewhat lower than the experimentally obtained value 0.994 [16,20].

2.3.4. Sm-*A*–Sm-*C* phase transition

A well-defined Smectic-*C* phase is illustrated by an inclined orientation of the molecular long axes at an angle θ with respect to the layer normal, *i.e.*, the density wave of the smectic phase is tilted with respect to the orientational axis [87,89]. This phase may appear in the system of molecules which have the broken axial symmetry. Several experimental studies suggest that there exist a secondary axis which is associated with the molecular permanent electric dipoles and aligned in a direction different from the typical long axis of the

molecules. According to the mean-field theory, in absence of the broken axial symmetry, the LC system with smectic-*C* phase behaves like a usual smectic-*A* phase and at this circumstance, it is important to observe how the off-axis dipole may produce such a tilt angle θ. These mean field theories [86], assumed the structure of a Landau theory with θ or sin θ as order parameter and the molecular model is used to determine the sign of the coefficients in the expansion of the free energy in powers of the order parameter.

However, the order parameter of the Sm-*C* phase is more complicated because the complete description of the molecular orientation requires not only the tilt angle θ with respect to the layer normal but also with an azimuthal angle φ of the axial direction for the molecules. Thus, the complex form of the order parameter can be written as [90,91]:

$$\omega = \theta \exp(i\varphi) = \omega_x + i\omega_y \tag{2.55}$$

According to Landau theory [81,82,86], the free energy density of the system can be expressed as a power series in terms of the relevant order parameter (in this case ω) in the vicinity of Sm-*A*–Sm-*C* phase transition. de Gennes [90-92] further modified this expression by including the concept of small fluctuation of ω close to that transition and reconsidered the power series as follows [93]:

$$f_n = f_0 + a|\omega|^2 + \frac{1}{2}b|\omega|^4 \tag{2.56}$$

where f_n and f_0 are the free energy density of the Sm-*C* and Sm-*A* phases respectively, while *a* and *b* are the temperature dependent constants. By using this free energy density expression, de Gennes [90-92] proposed a model that successfully describes a continuous or second order nature of the Sm-*A*–Sm-*C* phase transition analogous to the λ transition in superfluid helium (^{4}He). From this analogy some results have been obtained:

(i) The Sm-*A*–Sm-*C* phase transition should belongs to a continuous transition if the specific heat capacity data exhibits a singularity at the Sm-*A*–

Sm-*C* phase transition temperature (T_{AC}), *i.e.*, it follows the relation $\delta C_P \cong A + B^{\pm}|\tau|^{-\alpha}$, where *A*, *B* are constants, $\tau = (T - T_{AC})/T_{AC}$ and $\alpha \approx -0.007$.

(ii) For the temperature below the transition temperature T_{AC}, the tilt angle θ obey the relation $\theta \sim \theta_0|\tau|^{\beta}$, with the exponent $\beta = 1/3$, susceptibility follows $\chi \sim \chi_0|\tau|^{\gamma}$ with the value $\gamma = 1.33$ and correlation length also follows as $\xi \sim \xi_0|\tau|^{\nu}$ with ν = 0.67 where θ_0, χ_0 and ξ_0 are the parameters in the Sm-*A* phase.

(iii) For the temperatures above the transition temperature T_{AC}, an induced tilt angle appears by applying magnetic field *H* or electric field *E* to an oblique direction.

Additionally, Huang and Viner [94,95] proposed that the power series expansion contains the even ordered terms and at least up to sixth order term to explain the transitional behavior of the Sm-*A*–Sm-*C* phase transition and the free energy expression can be written as:

$$f_n = f_0 + a\tau|\omega|^2 + b|\omega|^4 + c|\omega|^6 \qquad (2.57)$$

where *a*, *b*, *c* are the temperature dependent positive constants and $\tau = (T - T_{AC})/T_{AC}$. T_{AC} is the Sm-*A*–Sm-*C* phase transition temperature. Hence, by imposing the free energy minimization condition, one can get:

(i) $\omega = 0$ for the Sm-*A* phase when $T > T_{AC}$ or $\tau > 0$,

(ii) $\omega^2 = \frac{b}{3c}\left[\left(1 + \frac{3\tau}{\tau_0}\right)^{1/2} - 1\right]$ for the Sm-*C* phase when $T < T_{AC}$ or $\tau < 0$

where $\tau_0 = \frac{b^2}{ac}$. Now, applying the obtained values into Eq. (2.57), the heat capacity expression can be written as:

$$C_P = -T\frac{\partial^2 f}{\partial T^2} \qquad (2.58)$$

Corresponding heat capacity values in the Sm-*A* and Sm-*C* phases can be described as:

$$C_P = C_0, \qquad \text{for } T > T_{AC} \text{ or } \tau > 0 \qquad (2.59)$$

$$C_P = C_0 + A'T(T_m - T)^{-1/2}, \quad \text{for } T < T_{AC} \text{ or } \tau < 0 \qquad (2.60)$$

where C_0 is the background heat capacity obtained from f_0 and $A' = a^{3/2}/[2(3c)^{1/2}{T_{AC}}^{3/2}]$, provided $T_m = T_{AC}(1 + \tau_0/3)$.

Now, in the vicinity of Sm-*A*–Sm-*C* phase transition point $\tau = 0$ and thus the discontinuity in heat capacity value becomes:

$$\Delta C_P = C_P - C_0 = \frac{a^2}{2bT_{AC}} \quad \text{for } T = T_{AC} \qquad (2.61)$$

when $\tau = -\tau_0$, Eq. (2.64) yields

$$\frac{C_P - C_0}{T} = \frac{a^2}{4b{T_{AC}}^2} = \frac{1}{2}\frac{\Delta C_P}{T_{AC}} \qquad (2.62)$$

This τ_0 represents the full width at half maxima of the $(C_P\text{-}C_0)/T$ vs. T curve in the reduced temperature scale.

However, $\tau_0 = \frac{b^2}{ac}$, it means that the order of the transition depends upon the values of coefficients *a*, *b* and *c*. According to the prediction of deGennes, the sixth ordered term *c* in Eq. (2.57) must be positive, *i.e.*, greater than 0, but if the value of *b* is negative ($b < 0$) the Sm-*A*–Sm-*C* phase transition demonstrates a first order nature, while if $b > 0$ results in a second order transition and when $b = 0$, a tricritical point appears where the Sm-*A*–Sm-*C* phase transition exhibits a crossover from second order to first order in nature. Therefore, in case of second order transition the value of τ_0 is too large ($|\tau| << \tau_0$) if $b >> c$ at the transition point and it reveals, $\omega \propto \tau^{1/2}$ as seen from the solutions of Eq. (2.57). However, at the tricritical point, $b \sim c > 0$ and τ_0 assumes a small value ($|\tau| >> \tau_0$) even for the temperatures close to the Sm-*A*–Sm-*C* phase transition. At the tricritical point, the solution approaches as $\omega \propto \tau^{1/4}$. Thus, this $|\tau|$ or τ_0 value defines the crossover behavior from mean field to tricritical nature of the Sm-*A*–Sm-*C* phase transition.

Nevertheless, the phenomenological Ginzburg-Landau theory [96-99] imparts a significant influence in describing the true critical phenomena for both classical and quantum statistical mechanics. Landau theory is a

straightforward macroscopic theory in a framework of statistical mechanics which is based on the concept that an average field is experienced by the non-interacting molecules within the system and hence ignores the effect of fluctuations. These mean field approximations are satisfactorily acceptable to describe the phase transitional phenomena in different thermodynamical systems having dimension d ≥ 4, but found to inadequate in low dimensional case (d < 4), which is further explained by Ginzburg. For example, in case of d > 4, the critical exponent β represents a value 0.5 predicted by the mean field approximation, while it assumes a bit different value 1/8 and 0.315, for two-dimensional (d = 2) and three-dimensions (d = 3) respectively. It suggests that there must be a certain limit of microscopic length scale over which the fluctuations of degrees of freedom are correlated. This length is termed as correlation length (ξ) which varies with temperature and serves as a scale for all distances. This ξ is connected to many particles of the system and the fluctuation of ξ near the transition point plays a role to determine the transitional phenomena. For a second-order phase transition, the correlation length becomes infinite, although it represents a finite value for a first-order transition. The parameter ξ is correlated over distances $\xi >> a$ (a is the intermolecular spacing) and diverges in close vicinity to the second order transition, *i.e.*, it follows the relation

$$\xi_{\pm} \propto |\tau|^{-\nu_{\pm}} \text{ or } \xi_{\pm} = \xi_0 |\tau|^{-\nu_{\pm}} \tag{2.63}$$

where ξ_0 is the range of interaction or the bare correlation length that can be measured directly from scattering studies and $\nu_+ = \nu_- = \nu = 1/2$. Therefore, the influence of correlation length is a crucial parameter near critical points which is considered to develop an adequate understanding how close to the transition temperature, Landau theory can explain the true critical phenomena. By proposing the free energy functional expression in terms of a wave function (ψ) as a complex order parameter, Ginzburg describes the fluctuation effect on the saddle point or mean field behavior for both the condition $\tau < 0$ and $\tau > 0$. He

introduces a correction term to the free energy expression regarding the dependency of the correlation length in which the integral term [100,101] is proportional to (length)$^{4-d}$. Mathematically, the fluctuation correlation term in heat capacity expression is expressed as:

$$C_{Fluct} \simeq \frac{1}{K^2}\begin{cases} a^{4-\mathrm{d}} & \text{for d} > 4 \\ \xi^{4-\mathrm{d}} & \text{for d} < 4 \end{cases} \qquad (2.64)$$

where K is the Hook's constant ($K \propto \xi_0^2$). The obtained results demonstrate that if d > 4, the correlation integral term diverges close to the transition temperature provided by an upper cutoff equal to $1/a$ (a = lattice spacing) as indicated in Fig. 2.11(a). However, the discontinuity in heat capacity value remains unchanged in the vicinity of the transition. Conversely, for d < 4, the correction term corresponds to the divergence of fluctuation ($\xi = \xi_0 |\tau|^{-1/2}$) and then the correlation integral reveals a convergent behavior. Effectively, the heat capacity value diverges close to the transition, implying that the mean field approximation fails to explain the true critical phenomena for the dimension d ≤ 4, which is called the upper critical dimension [101]. Now, imposing the condition $\xi = \xi_0 |\tau|^{-1/2}$ and $K \propto \xi_0^2$ into Eq. (2.64), the correction term modifies to ${\xi_0}^{-d}|\tau|^{-(\frac{4-d}{2})}$ which is greater than C_P in the mean field approximation.

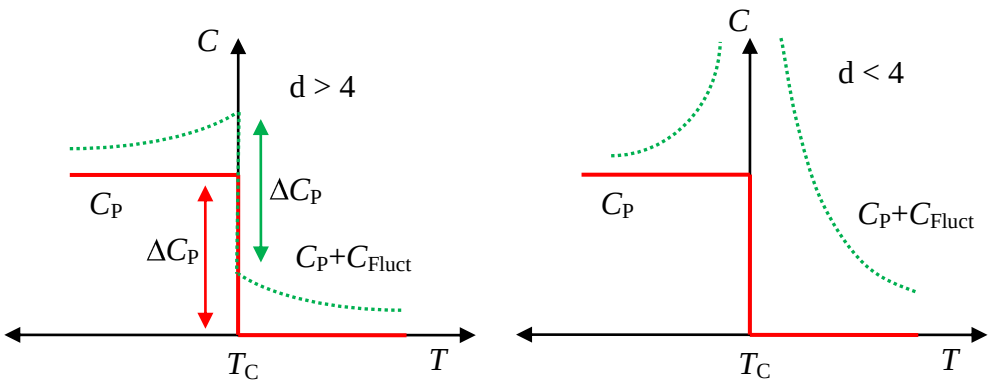

(a) (b)

Figure 2.11. Schematic diagram of the heat capacity variation near the phase transition for the dimensions d > 4 and d < 4. Red solid line is the mean field heat capacity and green dashed line corresponds to the same including the correction term appears due to the fluctuation of the correlation length.

Therefore, the fundamental expression of Ginzburg criterion can be written as

$$|\tau| \ll \tau_G \approx \frac{1}{[(\xi_0)^d(\Delta C_P)]^{2/(4-d)}} \tag{2.65}$$

where ΔC_P is the discontinuity in heat capacity obtained from mean field approximation. However, ξ_0 is the microscopic length scale which can be measured from scattering line shapes and τ_G is the Ginzburg reduced temperature. The correlation length ξ_0 is of the order of intermolecular spacing (a) and ΔC_P can be expressed as Nk_B. Thus the yielded value of the Ginzburg temperature in d = 3 is $\tau_G \approx \xi_0^{-5}$ [100]. In case of superconductor where $\xi_0 = 10^3 a$, τ_G demonstrates a value ~10^{-18} which is inaccessible by experimental techniques, while in superfluids it represents a value 10^{-1}–10^{-2}. Moreover, it has been observed that the region 10^{-2}–10^{-3} is hardly accessible by certain experimental techniques [95,102].

Based on the fundamental theories discussed above regarding the mesophase transition, it is clearly understood that the mean field theories are nothing but an approximation which omits the fluctuating order parameter and considers only the effect of the spatially uniform order parameter. Moreover, the mean field theory induces itself to its own self-consistency behavior and does not describe the dependency of transitional behavior upon the spatial dimension of the system. Practically, the mean field theory is only valid for the temperatures far away from the transition temperature. In case of the systems having a dimension less than 4 (d < 4), the mean field approximations are inadequate to describe the transitional behavior close to the transition point due to the divergence nature of correlation length fluctuation. As a result, the response function (like specific heat capacity) describes a power law divergence nature in the vicinity of transition temperature. Now, due to the failure of mean field theory and leading to an introduction of correlation length fluctuation, experimental observation of scaling and universality is more interesting close to the transition point. Owing to the divergence behavior of

correlation length in the vicinity of critical point, all the thermodynamical functions (free energy, specific heat capacity, susceptibility etc.) diverges according to the correlation length. Furthermore, the singularity of a phase transition in any thermodynamical observables is characterized by a critical exponent like as α, β, γ etc. which are not independent to each other. Hence, there must be a correlation to each other for the exponents as well as the thermodynamic functions which depend upon the temperature that is nailed as scaling behavior. This relationship between the observables and related exponents in the vicinity to a phase transition point can be well described by the power-law divergence near the transition temperature. The singularities of different physical properties can be estimated by the divergence behavior of ξ at T_C. Moreover, the singularities or scaling condition in free energy expression can be described by a single generalized homogeneous function of temperature and conjugate field and represented as:

$$f(\tau, h) = |\tau|^2 g(h/|\tau|^{\Delta}) \tag{2.66}$$

where h is the externally applied field, Δ is the gap exponent and g is the homogeneous function dependent upon h and τ. However, considering the homogeneity, the singular form of free energy assumes an expression

$$f'(\tau, h) = |\tau|^{2-\alpha} g(h/|\tau|^{\Delta}) \tag{2.67}$$

Hence the singular form of the energy becomes

$$E'(\tau, h) \sim \frac{\partial f'}{\partial \tau} = |\tau|^{1-\alpha} g_E(h/|\tau|^{\Delta}) \tag{2.68}$$

and similarly, the singular form of heat capacity becomes

$$C'(\tau, h) \sim \frac{\partial^2 f'}{\partial \tau^2} = |\tau|^{-\alpha} g_C(h/|\tau|^{\Delta}) \tag{2.69}$$

or it may be expressed more generalized way as

$$C_{\pm}(\tau, h) = |\tau|^{-\alpha_{\pm}} g_{C_{\pm}}(h/|\tau|^{\Delta_{\pm}}) \tag{2.70}$$

with separate values of function and exponent for $\tau < 0$ and $\tau > 0$ that coincide at $\tau = 0$. However, at $h = 0$, Eq. (2.70) yields

$$C_{\pm}(\tau, 0) = A|\tau|^{-\alpha_{\pm}} \tag{2.71}$$

where A is the amplitude coefficient. On the other hand, the correlation length ξ is a homogeneous function that can be expressed as

$$\xi(\tau, h) = |\tau|^{-\nu} g(h/|\tau|^{\Delta}) \tag{2.72}$$

Thus the singular form of the free energy function reveals

$$f'(\tau, h) \sim \xi^{-d} \sim |\tau|^{d\nu} g(h/|\tau|^{\Delta}) \tag{2.73}$$

Comparing Eq. (2.67) and Eq. (2.73), one can get the relation $2 - \alpha = d\nu$ or $\alpha = 2 - d\nu$ which is named as Joshephson's equality or identity. Similarly there are some other relations and these relations are a result of the homogeneity or scaling properties of correlation functions and thermodynamic quantities near $T = T_c$ that can be derived using the renormalization group model introduced by Kenneth Wilson [103-105]. This procedure is based on the three concept- Coarse graining, Rescaling and Renormalization, explored that the critical exponents are dependent upon the spatial dimension, symmetry of the order parameter and symmetery as well as range of interactions. They belong to some universality classes in which the critical exponents for all the transitions is identical.

After the above theoretical discussions, it is obvious that the microscopic behavior at the critical point can be well reflected by the response functions such as specific heat capacity, susceptibility, magnetization etc. According to the mean field model the quantity (S-S_0) is proportional to $\langle|\Psi|^2\rangle$, where S_0 is the nematic order parameter in absence of any smectic ordering [91,106]. Moreover, the nematic order parameter (S) is also proportional to optical birefringence (Δn). Hence, by investigating the behavior of optical birefringence in the vicinity of transitions between liquid crystal mesophases, an identical power-law divergence behavior and hence a critical

exponent (α') identical to specific heat critical exponent (α) can be established. Most of the experimental part in this dissertation is mainly concentrated on determining the mesophase transitional behavior and their order character by investigating the temperature dependent optical birefringence measurement.

References:

[1] D. Demus, and L. Richter, in *Textures of liquid crystals*, Verlag Chemie, New York (1978).

[2] I. Dierking, in *Textures of liquid crystals*, Wiley-VCH Verlag GmbH & Co., Weinheim (2003).

[3] P. Navard, and J. M. Haudin, *J. Therm. Anal.*, **30**, 61 (1985).

[4] C.W. Garland, in *Liquid Crystals: Experimental Study of Physical Properties and Phase Transitions*, S. Kumar (Ed.), Cambridge University Press, Cambridge (2001).

[5] J. Thoen, in *Heat Capacities Liquids, Solutions and Vapours*, E. Wilhelm, and T. M. Letcher (Eds.), RSC Publishing, Cambridge (2010).

[6] R. Dabrowski, and K.C. Zuprynski, in *Advances in liquid crystal research and applications*, Pergamon press, Oxford (1980).

[7] H. Stub, and W. Perron, *Anal. Chem*., **46**, 128 (1974).

[8] B. Das, A. Pramanik, M.K. Das, A. Bubnov, V. Hamplová, and M. Kašpar, *J. Mol. Struct.*, **1013**, 119 (2012).

[9] B.R. Ratna, and S. Chandrasekhar, *Mol. Cryst. Liq. Cryst.*, **162**, 157 (1988).

[10] A.K. Zeminder, S. Paul, and R. Paul, *Mol. Cryst. Liq. Cryst.*, **61**, 4191 (1980).

[11] A. Prasad, and M.K. Das, *Phase Transitions*, **83**, 1072 (2010).

[12] A. Saipa, and F. Giesselmann, *Liq. Cryst.*, **29**, 347 (2002).

[13] T. Scharf, in *Polarized Light in Liquid Crystals and Polymers*, John Wiley and Sons, Hoboken (2007).

[14] G. Sarkar, B. Das, M.K. Das, and W. Weissflog, *Phase Transiions*, **82**, 433 (2009).

[15] A. Prasad, and M.K. Das, *J. Phys.: Condens. Matter*, **22**, 195106 (2010).

[16] S.K. Sarkar, and M.K. Das, *RSC Adv.*, **4**, 19861 (2014).

[17] G. Sarkar, M.K. Das, R. Paul, B. Das, and W. Weissflog, *Phase Transit*., **82**, 433 (2009).

[18] S.K. Sarkar, P.C. Barman, and M.K. Das, *Physica B*, **446**, 80 (2014).

[19] S.K. Sarkar, and M.K. Das, *J. Mol. Liq.*, **199**, 415 (2014).

[20] A. Chakraborty, S. Chakraborty, and M.K. Das, *Phys. Rev. E*, **91**, 032503 (2015).

[21] M.K. Das, S. Chakraborty, R. Dabrowski, and M. Czerwinski, *Phys. Rev. E*, **95**, 012705 (2017).

[22] A. Saipa, and F. Giesselmann, *Liq. Cryst.*, **29**, 347 (2002).

[23] T. Scharf, in *Polarized Light in Liquid Crystals and Polymers*, John Wiley and Sons, Hoboken (2007).

[24] A. Prasad, and M.K. Das, *Phys. Scr.*, **84**, 015603 (2011).

[25] A. Chakraborty, M.K. Das, B. Das, U. Baumeister, and W. Weissflog, *J. Mater. Chem. C*, **1**, 7418 (2013).

[26] S.K. Sarkar, and M.K. Das, *Fluid Phase Equilib*., **365**, 41 (2014).

[27] S.K. Sarkar, and M.K. Das, *Liq. Cryst.*, **41**, 1410 (2014).

[28] P. Galatola, and C. Oldano, in *The Optics of Thermotropic Liquid Crystals*, S. Elston, and R. Sambles (Eds.), Tailor and Francis, London (1998).

[29] P. Perkowski, M. Mrukiewicz, K. Garbat, M. Laska, U. Chodorow, W. Piecek, R. Dabrowski, and J. Parka, *Liq. Cryst.* **39**, 1237 (2012).

[30] M. Mrukiewicz, P. Perkowski, K. Garbat, R. Dabrowski, and J. Parka, *Acta Physica Polonica A*, **124**, 940 (2013).

[31] S. Havriliak, and S. Negami, *Polymer*, **8**, 161 (1967).

[32] S. Havriliak, and S. Negami, *J. Poly. Sci.*, **14**, 99 (1966).

[33] P. Nayek, S. Ghosh, S.K. Roy, T.P. Majumder, and R. Dabrowski, *J. Mol. Liq.* **175**, 91 (2012).

[34] S. Ghosh, P. Nayek, S.K. Roy, T. P. Majumder, and R. Dabrowski, *Liq. Cryst.*, **37**, 369 (2010).

[35] D.W. Davidson, and R. H. Cole, *J. Chem. Phys.* **19**, 1484 (1951).

[36] K.S. Cole, and R.H. Cole, *J. Chem. Phys*, **9**, 341 (1941).

[37] F.C. Frank, *Disc. Faraday Soc.*, **25**, 19 (1958).

[38] C.W. Oseen, *Trans. Faraday Soc.*, **29**, 883 (1933).

[39] H. Zocher, *Trans. Faraday Soc.*, **29**, 945 (1933).

[40] W.H. de Jue, in *Physical Properties of Liquid Crystalline Materials*, Gordon and Breach, London (1980).

[41] S. Chandrasekhar, in *Liquid Crystals*, Cambridge University Press, Cambridge (1992).

[42] M. Kleman, in *Points, Lines and Walls*, Wiley, New York (1983).

[43] P.G. de Gennes, and J. Prost, in *The Physics of Liquid Crystals*, Oxford University Press, Oxford (1993).

[44] S. Singh, in *Liquid Crystals Fundamentals*, World Scientific, Singapore (2002).

[45] V. Fréedericksz, and V. Zolina, *Trans. Faraday Soc*., **29**, 919 (1933).

[46] H.L. Ong, *Phys. Rev. A*, **33**, 3550 (1986).

[47] M.J. Bradshaw, and E.P. Rayens, *Mol. Cryst. Liq. Cryst.*, **72**, 35 (1980).

[48] H. Deuling, in *Liquid crystals, Solid state physics suppl. no. 14*, L Liebert, (Ed), Academic Press, New York (1978).

[49] H. Gruler, T.J. Scheffer, and G. Meier, *Z. Naturforsch.*, **27a**, 966 (1972).

[50] H. Gruler, and L. Cheung, *J. Appl. Phys.*, **46**, 5097 (1975).

[51] L. Pohl, and U. Finkenzeller, in *Liquid Crystals – Applications and Uses*, B. Bahadur (Ed.), World Scientific, Singapore (1990).

[52] P.P. Karat, and N.V. Madhusudana, *Mol. Cryst. Liq. Cryst.*, **40**, 239 (1977).

[53] H.P. Schad, G. Baur, and G. Meier, *J. Chem. Phys.*, **70**, 2770 (1979).

[54] M.J. Bradshaw, and E.P. Raynes, *Mol. Cryst. Liq. Cryst.*, **72**, 35 (1981).

[55] H.P. Schad, and M.A. Osman, *J. Chem. Phys.*, **75**, 880 (1981).

[56] F. Leenhouts, and A.J. Dekker, *J. Chem. Phys.*, **74**, 1956 (1981).

[57] L. Csillag, I. Jánossy, V.F. Kitaeva, N. Kroó, N. Sobolev, and A.S. Zolotko, *Mol. Cryst. Liq. Cryst.*, **78**, 173 (1981).

[58] A. Chakraborty, M.K. Das, B. Das, A. Lehmann, and C. Tschierske, *Soft Matter*, **9**, 4273 (2013).

[59] A. Prasad, and M.K. Das, *Liq. Cryst.*, **41**, 1261 (2014).

[60] P. Sathyanarayana, T.A. Kumar, V.S.S. Sastry, M. Mathews, Q. Li, H. Takezoe, and S. Dhara, *Appl. Phys. Exp.*, **3**, 091702 (2010).

[61] S. Das Gupta, P. Chattopadhyay, and S.K. Roy, *Phys. Rev. E.*, **63**, 041703 (2001).

[62] S. Das Gupta, and S.K. Roy, *Liq. Cryst.*, **30**, 31 (2003).

[63] E. Jakeman, and E.P. Raynes, *Physics Lett. A*, **39**, 69 (1972).

[64] Hp. Schad, *J. Appl. Phys.*, **54**, 4994 (1983).

[65] P. Martinot-lagarde, *J Phys. Lett.* (*Paris*), **38**, 17 (1977).

[66] K. Miyasato, S. Abe, H. Takezoe, A. Fukuda, and E. Kuze, *Jpn. J Appl. Phys.*, **22**, L661 (1983).

[67] S.S. Bawa, A.M. Biradar, K. Saxena, and S. Chandra, *Rev. Sci. Instrum.*, **59**, 2023 (1988).

[68] A. Pramanik, M.K. Das, B. Das, M. Żurowska, and R. Dabrowski, *Liq. Cryst.*, **42**, 412 (2015).

[69] V.M. Vaksman, and Y.P. Panarin, *Mol. Mats*., **1**, 147 (1992).

[70] W. Maier, and A. Saupe, *Z. Natureforsch A*, **13a**, 564 (1958).

[71] W. Maier, and A. Saupe, *Z. Natureforsch A*, **14a**, 882 (1959).

[72] W. Maier, and A. Saupe, *Z. Natureforsch A*, **15a**, 287 (1960).

[73] S. Chandrasekhar, in *Liquid crystals*, Cambridge University Press, Cambridge (1977).

[74] G.R. Luckhurst, G.W. Gray (Eds), in *The molecular physics of liquid crystals*, Academic Press, London (1979).

[75] W.L. McMillan, *Phys. Rev. A*, **4**, 1238 (1971).

[76] W.L. McMillan, *Phys. Rev. A*, **6**, 936 (1972).

[77] K. Kobayashi, *J. Phys. Soc. Jpn.*, **29**, 101 (1970).

[78] K. Kobayashi, *Mol. Cryst. Liq. Cryst.*, **13**, 137 (1971).

[79] K. Kobayashi, *Phys. Lett. A*, **31**, 125 (1970).

[80] P.J. Wojtowlcz, in *Introduction to Liquid Crystals,* E. B. Priestley, P. J. Wojtowicz and P. Sheng (Eds.), Plenum Press (1976).

[81] L.D. Landau, *Phys. Z Sowjefunion*, **11**, 26 (1937); in *Collected papers of L.D. Landau*, D. Ter Haar (2nd Ed.), Gordon and Breach, Science Publisher, New York (1967).

[82] L.D. Landau, and E.M. Lifshitz, in *Statistical Physics* (Vol. 1, 3rd Ed.), Pergamon, Oxford (1980).

[83] P.G. de Gennes, *Mol. Cryst. Liq. Cryst.*, **12**, 193 (1971).

[84] E.B. Priestly, P.J. Wojtowicz, and P. Sheng (editors), in *Introduction to Liquid Crystals* (Ch. 10), Plenum Press, New York (1975).

[85] S. Singh, *Phys. Rep.*, **324**, 107 (2000).

[86] G. Vertogen, W.H. de Jeu, in *Thermotropic liquid crystals: Fundamentals*, Springer, Berlin (1988).

[87] P.G. de Gennes, in *The Physics of Liquid Crystals*, Clarendon Press, Oxford (1974).

[88] M.A. Anisimov, in *Critical phenomena in liquids and liquid crystals*, Gordon and Breach, New York (1991).

[89] J.D. Litster, and R.J. Birgeneau, *Phys. Today*, **35**, 26 (1982).

[90] P.G. de Gennes, *Solid State Comm.*, **10**, 753 (1972).

[91] P.G. de Gennes, *Mol. Cryst. Liq. Cryst.*, **21**, 49 (1973).

[92] P.G. de Gennes, *C. R. Acad. Sci. B*, **274**, 758 (1972).

[93] M.J. Stephen, and J.P. Straley, *Rev. Mod. Phys.*, **46**, 617 (1974).

[94] C.C Huang, and J.M. Viner, *Phys. Rev. A*, **25**, 3385 (1982).

[95] S.C. Lien, and C.C. Huang, *Phys. Rev. A*, **30**, 624 (1984).

[96] V. L. Ginzburg, *Sov. Phys. - Solid State*, **2**, 1824 (1961).

[97] J. Als-Nielsen, and R.J. Birgeneau, *Am. J. Phys.*, **45**, 554 (1977).

[98] N. Goldenfeld, in *Lectures on phase transitions and the renormalization group*, Talor & Francis group, NW (1992).

[99] D.J. Amit, *J. Phys. C: Solid State Physics*, **7**, 3369 (1974).

[100] P.M. Chaikin, and T.C. Lubensky, in *Principles of condensed matter physics*, Cambridge University Press, New York (1995).

[101] M. Kardar, in *Statistical physics of field*, Cambridge University Press, New York (2007).

[102] G. Ahlers, A. Kornblit, and H.J. Guggenheim, *Phys. Rev. Lett.*, **34**, 1227 (1975).

[103] K.G. Wilson, in *An investigation of the low equation and the Chew-Mandelstam equations*, Ph.D thesis, Cal. Tech. (1961).

[104] K.G. Wilson, *Rev. Mod. Phys.*, **55**, 583 (1983).

[105] K.G. Wilson, and J. Kogut, *Phys. Rep.*, **12**, 75 (1974).

[106] K.-C. Lim, and J.T. Ho, *Phys. Rev. Lett.*, **40**, 944 (1978).